Journal of Energy Chemistry 27 (2018) 673–689

Contents lists available at ScienceDirect

Journal of Energy Chemistry

journal homepage: www.elsevier.com/locate/jechem

http://www.journals.elsevier.com/journal-of-energy-chemistry/

Review

Recent advances of flexible perovskite solar cells

Lingbo Li[a,b], Shasha Zhang[a], Zhichun Yang[a], Engamba Esso Samy Berthold[b], Wei Chen[a,c,*]

[a] Wuhan National Laboratory for Optoelectronics, Huazhong University of Science and Technology, Luoyu Road 1037, Wuhan 430073, Hubei, China
[b] China-EU Institute for Clean And Renewable Energy, Huazhong University of Science and Technology, Luoyu Road 1037, Wuhan 430073, Hubei, China
[c] Engineering Research Center of Nano-Geo Materials of Ministry of Education, China University of Geosciences, Wuhan 430074, Hubei, China

ARTICLE INFO

Article history:
Received 19 October 2017
Revised 2 January 2018
Accepted 8 January 2018
Available online 11 January 2018

Keywords:
Perovskite solar cell
Flexible solar cell
Low-temperature process
Roll-to-roll manufacture
Thin film encapsulation

ABSTRACT

In few years only, the efficiency record of perovskite solar cells (PSCs) has raised quickly from 3.8% to over 22%. This emerging photovoltaic technology has primarily shown its great potential of industrialization. Flexible PSCs are thought to be one of the most priority options for mass production, related to the intrinsic advantage of perovskite thin films which could be deposited by facile solution processes at low temperature. Flexible PSCs have at least four advantages in comparison to the rigid counterpart: (1) it can generate higher power output at lighter weight, (2) it is easily portable, (3) it can be easily attached to architectures or textiles with diverse shapes, and (4) it is compatible with roll-to-roll fabrication in a large scale. In this review, we have summarized recent development of the key materials and technologies applied in flexible PSCs. The key materials including flexible substrates, transparent and conductive electrodes, and interfacial materials; some key technologies about roll-to-roll manufacture, encapsulation technology have been overviewed. Finally, a prospect on possible application directions of flexible PSCs has been discussed.

Lingbo Li is currently a M.S. candidate under supervision of Prof. Wei Chen at Wuhan National Laboratory for Optoelectronics and China-EU Institute for Clean and Renewable Energy, Huazhong University of Science and Technology. She received her B.S. degree from Department of Mathematics and Physics, Suzhou University of Science and Technology in 2016. Her research focuses on flexible perovskite solar cells.

Shasha Zhang received her Ph.D. degree in Material Science from Huazhong University of Science and Technology in 2016. She currently is a postdoctoral fellow at Wuhan National Laboratory for Optoelectronics, Huazhong University of Science and Technology. Her research activities focus on the charge transport mechanism and stability of perovskite solar cells.

Zhichun Yang obtained his B.S. degree in physics in 2014 from Yun Cheng University, China, and his M.S. degree in condensed matter physics in 2017 from Huazhong University of Science and Technology, China. He is currently a Ph.D. candidate at Wuhan National Laboratory for Optoelectronics, Huazhong University of Science and Technology. His research mainly focuses on large-area perovskite solar cells and modules.

Samy Berthold Engamba Esso is a MS candidate under the supervision of Prof. Wang Yi at the State Key Laboratory of Coal Combustion and China European Union Institute of Clean and Renewable Energy of the Huazhong University of Science and Technology. He graduated a master in industrial engineering from the National Advanced School of Engineering of Yaounde, Cameroon in 2014. He is leading some researches in the interaction of coal and biomass during the co-fast pyrolysis.

* Corresponding author at: Wuhan National Laboratory for Optoelectronics, Huazhong University of Science and Technology, Luoyu Road 1037, Wuhan 430073, Hubei, China.
E-mail address: wnlochenwei@mail.hust.edu.cn (W. Chen).

https://doi.org/10.1016/j.jechem.2018.01.003

Wei Chen received his B.S. and Ph.D. degree from Department of Materials Science and Engineering in Tsinghua University. He worked as postdoctoral fellowship in Department of Chemistry in Hong Kong University of Science and Technology from 2008 to 2010. He was a visiting scholar in National Institute for Materials Science in Japan from 2014 to 2015. He is currently a professor in Wuhan National Laboratory for Optoelectronics of Huazhong University of Science and Technology. His research interests cover the synthesis, understanding, and applications of functional nanomaterials and semiconductor thin films in next generation solar cells, including perovskite solar cells, dye and quantum dot-sensitized solar cells, and printable low-cost solar cells.

1. Introduction

Since the beginning of the new century, both of the world population and global energy demand keep on fast growing. However, most of the energy consumption still comes from fossil fuels. In addition to this, the environmental pollution and global warming problems become more and more urgent and cause extensive concern. To develop clean and renewable energies to replace conventional fossil fuels becomes an indispensable choice for human communities. Among kinds of renewables, solar energy is the most abundant one and less dependent on geographical location. Photovoltaic solar cells directly convert solar light into electricity and are one of the most effective ways to utilize the clean and renewable solar energy. According to UNECE Renewable Energy Status Report, the capacity of global photovoltaic installation is continually increasing, which has reached 227 GW at the end of 2015 (Fig. 1) [1]. However, in comparison to the total solar energy reaching the earth's surface, 227 GW is nearly negligible.

To realize further scale-up utilization of solar energy, the primary issue is to reduce the levelized cost of electricity for solar cells to be more competitive comparing to fossil fuels. The fabrication of photovoltaic devices on flexible substrates could dramatically lower down the processing cost, by introducing high-throughput roll-to-roll manufacturing and low-temperature energy-saving technological processes. In comparison to the rigid counterpart, flexible solar cells are lightweight, bendable, and convenient for transportation and installation. Accordingly, they can be easily applied in "building integrated photovoltaics" and wearable electricity-generating devices. However, many new obstacles could be aroused for flexible solar cells. For example, most of the flexible substrates made of plastic materials cannot sustain high temperature treatment, therefore, the processing temperature has to be controlled under 150 °C. And at such low temperature range, electrical and mechanical properties of many semiconductor films cannot be sufficiently optimized, leading to poor performance of the devices. Besides, many plastic substrates in comparison to rigid glass substrates have higher water vapor and oxygen transmission rates [2], generally leading to fast degradation of the active films and poor long-term stability of the flexible devices.

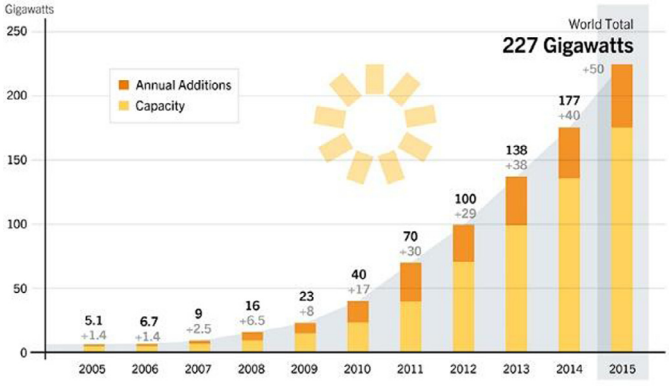

Fig. 1. Capacities and annual additions of global photovoltaic installations from 2005 to 2015 [1]. Reproduction from ref. [1] with the permission from Renewable Energy Policy Network for the 21st Century.

The first generation of silicon-based solar cells has intrinsic rigid property. Bending with radius less than 10 cm can lead to performance deterioration of the modules [3]. Strip-shaped, electrically-interconnected silicon-based solar modules were reported to have a certain flexibility, however, high cost and complex manufacturing were induced in the mean time [4]. The second generation of thin film solar cells has a better flexibility. Among them, flexible GaAs and CIGS solar cells have achieved the best efficiencies up to 26.7% [5] and 20.4% [6], respectively. But the toxicity and scarcity of some imperative elements may limit their development in a large scale. Some of the third generation solar cells could be made at even lower processing temperature, which could be benefit to the fabrication of flexible solar cells. The best flexible dye-sensitized solar cell has reached an efficiency of 8.6% [7]. The reported efficiencies of flexible organic solar cells (OPVs) have reached over 8% at small area [8] and over 4% at module scale with active area of 114.5 cm^2 [9].

As an emerging photovoltaic technology with fast developing speed, perovskite solar cells (PSCs) have attracted broad attention for the high efficiency, low-cost and solution-processible features. Flexible fabrication of PSCs will maximize its manufacture advantages and minimize the processing cost. Flexible PSCs are thought to have almost all of the positive characters of OPVs and their fabrication can mimic the mature craft of OPVs' fabrication to a large extent. The most important is the fact that, flexible PSCs can simply achieve much higher efficiency [10] than OPVs.

This review focuses on recent advances of the key materials, technological processes, encapsulation and applications of flexible PSCs. Section 2 starts with the low-temperature process characteristics of perovskite thin films and overviews the developing status of flexible PSCs. Sections 3 to 5 review the substrate materials, the transparent-conductive electrode materials, and the charge transport interfacial materials compatible with flexible PSCs. Section 6 introduces the roll-to-roll manufacturing processes adapted to flexible PSCs. Finally, Sections 7 and 8 extend to the thin film encapsulation technology and diverse applications of flexible PSCs.

2. Perovskite materials and performance development of flexible PSCs

2.1. Why perovskite materials are promising for flexible devices

The pristine "perovskite" represents a calcium titanium oxide mineral with the formula of $CaTiO_3$ which was firstly discovered by a Russia mineralogist in 1839 [11]. In a broad sense, perovskites stand for a class of compounds which have the same type of crystal structure as $CaTiO_3$. In 1980, for the first time, $KPbI_3$ and other halide perovskite materials have been suggested as potential photovoltaic materials because of suitable optical bandgaps [12]. However, the first practical PSCs were initiated by Miyasaka and coworkers in 2009. They demonstrated the prototype of photoelectrochemical cells with $CH_3NH_3PbBr_3$ and $CH_3NH_3PbI_3$ as sensitizers [13]. The ideal crystal structure of perovskite [14] is shown in Fig. 2(a), where A represents monovalent cations with large radius which usually are $CH_3NH_3^+$, $HC(NH_2)_2^+$, or Cs^+; B represents divalent cations which usually are Pb^{2+}, Sn^{2+}, or Ge^{2+}; and X represents halogen anions of I^-, Br^-, or Cl^-. Six BX_6 octahedrons through corner-sharing, together with a body-centered A cation, constitute the three-dimensional perovskite structure [15].

Among perovskite materials with different polymorphs, the cubic perovskites with high symmetry have better photoelectric

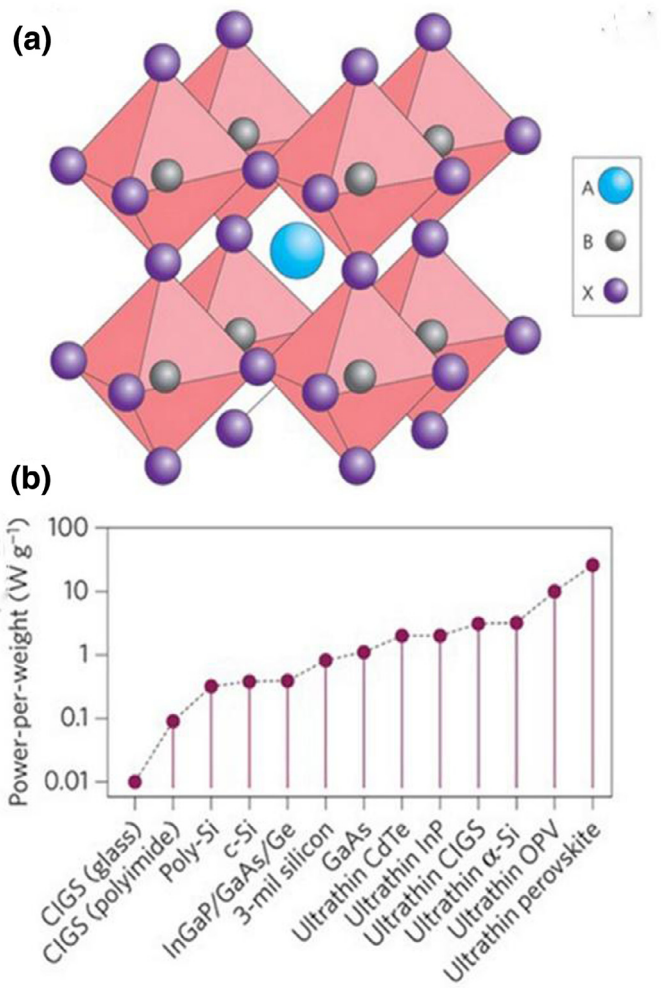

Fig. 2. (a) Ideal crystal structure of perovskites [14] (Reproduction from ref. [14] with the permission from Nature Publishing Group.), (b) comparison of leading light-weight solar cells from academic results [22] (Reproduction from ref. [22] with the permission from Nature Publishing Group).

Table 1. Cubic phase-transition temperatures of some frequently-reported perovskites [16,17].

Materials	Temperature (K)	Materials	Temperature (K)
$CH_3NH_3PbCl_3$	~179	$HC(NH_2)_2PbI_3$	~360
$CH_3NH_3PbBr_3$	~237	$CsPbBr_3$	~403
$CH_3NH_3PbI_3$	~327	$CsPbI_3$	~589

properties, which play a decisive role to the solar cells' performance. The phase-transition temperatures of some frequently-reported perovskite materials are shown in Table 1 [16,17]. The stable cubic phases are normally obtained at relatively lower temperature for the organic–inorganic hybrid perovskites in comparison to the fully inorganic perovskites. For example, the phase-transition temperature of $CH_3NH_3PbI_3$ is only 327 K, while that of $CsPbI_3$ is 589 K. This implies organic–inorganic hybrid perovskites are more compatible with flexible technology in comparison to the fully inorganic ones. Smooth and compact $CH_3NH_3PbI_3$ perovskite films have been obtained through spin-coating and annealing at about 100 °C [18,19], $HC(NH_2)_2PbI_3$ perovskite films have been obtained at about 150 °C [20], while $CsPbI_3$ perovskite films need to be annealed at 200–300 °C [21]. The low-temperature crystallization property of organic–inorganic hybrid perovskites constitutes the primary reason for the flexible fabrication of PSCs.

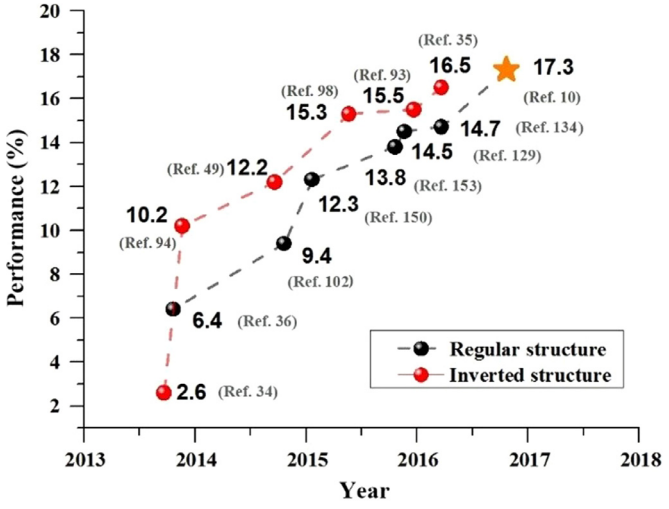

Fig 3. Performance evolution of flexible PSCs.

Secondly, for flexible fabrication of PSCs, the mechanical properties of perovskite films should also be taken into consideration. Based on the first principles, Feng [23] calculated the theoretical expectation on the flexibility of perovskite materials, which is determined by the chemical bond of B-X and the ratio of bulk modulus to shear modulus of perovskite materials. He pointed out that the ratio of over 2.0 allowed perovskite materials to endure compression, tortuosity and bending to some extent. Furthermore, suitable Poisson's ratio of perovskite materials ($\tau > 0.26$) also indicates their desirable flexibility. These mechanical properties might be the secondary reasons to support perovskites for flexible fabrication.

Thirdly, organic–inorganic hybrid perovskite materials are able to dissolve in organic polar solvents [24–27]. This allows high quality perovskite thin films to be deposited *via* simple solution processes, such as spin-coating [28,29], spray-coating [30], ink-jet printing [31], slot-die coting [32] and blade-coating [33]. Many of these film deposition techniques can be integrated into the roll-to-roll production line for the fabrication of flexible PSCs.

At last, direct bandgap perovskite materials have high light adsorption coefficient, allowing PSCs can be fabricated with ultrathin thickness without decreasing performance; and therefore, PSCs can achieve ultrahigh power-per-weight ratio. As shown in Fig. 2(b), the highest power-per-weight ratio of flexible PSCs reached 23 W/g which surpassed all of the other kind solar cells [22]. The ultrahigh power-per-weight ratio is prerequisite for some special applications, such as portable power sources for military unmanned aircraft in order to prolong the flight range.

2.2. Performance evolution of flexible PSCs

Fig. 3 shows the power conversion efficiency (PCE) evolution of flexible PSCs during recent years. The devices have been divided into two branches: one is with regular n-i-p structure and the other one with inverted p-i-n structure, according to different working principles and key materials' layouts. Regular structured devices with n-i-p layout employed n-type semiconductor as selective contact in the bottom to collect photo-generated electrons and transport them to the photoanode. In 2013, Mathews' group [34] reported the first flexible PSC with regular structure employing low-temperature deposited ZnO for electron collection, achieving a PCE of 2.64%. For a higher efficiency and stability, many other types of n-type electron selective interfacial layers, new perovskite materials and better quality control on perovskite thin films, and alternative transparent electrode materi-

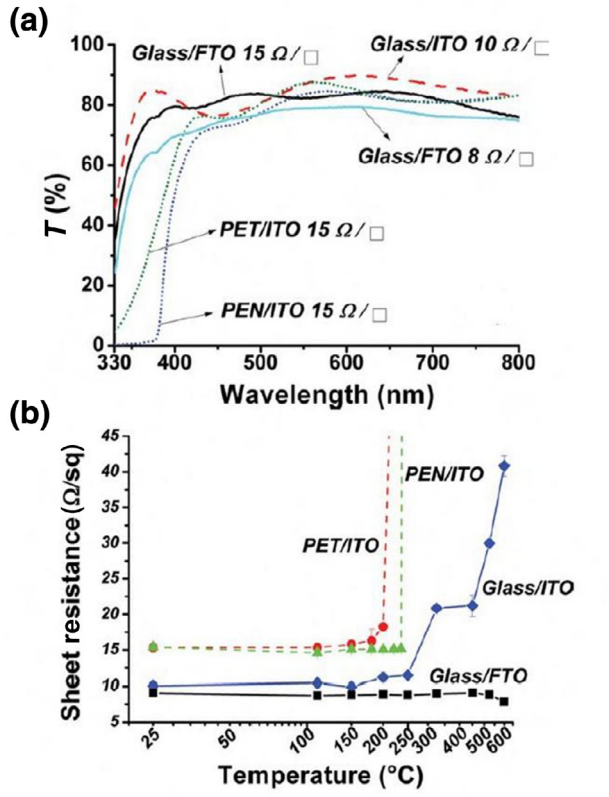

Fig. 4. (a) UV–vis transmittance spectra of glass/ITO, glass/FTO, PET/ITO and PEN/ITO substrates; (b) sheet resistance degradation of different substrates supported conductive layers under thermal treatment [37]. Reproduction from ref. [37] with the permission from Wiley.

als have been investigated in the following years. In 2016, Shin et al. [35] developed a Zn_2SO_4 nanoink which could be spin-coated as the electron transport layer. Based on the perovskite material of $CH_3NH_3Pb(I_{0.9}Br_{0.1})_3$, the flexible PSC achieved a PCE up to 16.5%, which is the highest for regular structured flexible PSCs until now. The research on flexible PSCs with inverted structure started relatively later but caught up quickly with the regular counterpart. Docampo et al. [36] proposed the prototype of inverted flexible PSCs, with poly(3,4-ethylene dioxythiophene): poly(styrene sulfonate) (PEDOT: PSS) and 6,6-phenyl C61-butyric acid methyl ester (PCBM) as the p-type and n-type charge selective interfacial layers respectively. The device achieved an efficiency of 6.4%. In 2016, Yoon et al. [10] developed CVD deposited graphere as photoanode, exhibiting a record-high efficiency of 16.8% with impressing flexibility. Moreover, the counterpart fabricated on ITO photoanode showed a higher effiency (17.3%), which is the highest for inverted flexible PSCs until now. As the further development of new materials and low-temperature techniques to control the films' quality, the efficiency record of flexible PSCs should be quickly improved to be over 20% in the near future.

3. Selection of flexible substrates

PSCs are normally fabricated on the rigid glass substrates, which have good optical transmittance, heat resistance, corrosion resistance and good contact with the transparent conductive films. The main drawbacks are its fragile nature and energy-intensive manufacturing. Polyethylene terephthalate (PET) and polyethylene naphthalate (PEN) films are promising flexible substrates because of their bendability, low-cost, deactivation to usual solvents and high optical transparency as shown in Fig. 4(a) [37]. However, the glass transition temperatures of PET and PEN are about 78 °C and 120 °C respectively. This largely hinders the end-use temperature up-limits of devices based on these plastic flexible substrates. In Fig. 4(b), after heated at 200 °C and 240 °C for 30 min respectively, the sheet resistances of PET/ITO and PEN/ITO conductive substrate got a significant increase. One of the plastic substrates which can bear relatively high temperature is polyimide (PI) with glass transition temperature of above 200 °C. PI has been used as substrates in flexible CIGS solar cells [6] which requires relatively high temperature processing. But conventional PI is light brown in color, which affects its optical transmittance. Recently, colorless PI film has also been fabricated and used as flexible substrate in PSCs. The transmittance and bendability of the reported PI/ITO film are even higher than that of the PET/ITO reference [38].

Another type of flexible substrates is metallic foils (Fig. 5(a)). In comparison to plastic substrates, metal foils normally have lower water vapor transmission rate, higher electric conductivity, and higher thermal endurance. Ti foils were frequently selected as substrates in flexible solar cells due to its excellent corrosion resistance and high strength-weight ratio. But metal is intrinsically opaque so that a transparent counter electrode is imperative for light entrance. In addition, when a conductive glass was used as the substrate, the conductive layer on glass could be etched by laser to avoid short circuit during its testing. Therefore, on a glass substrate, it is facile to design solar modules connected in series or in parallel. But it is difficult to fabricate solar modules connected in series on a metal substrate, because the electric connection of metal foil cannot be broken without physical separation [39]. Besides Ti foil, Cu [40] and stainless foils [41,42] have been also used as metal substrates in flexible PSCs. Some metallic photoanode with fibrous shape are extraordinary pliable, as shown in Fig. 5(b) and (c). These fiber-shaped PSCs can absorb solar light from all the incident directions. Furthermore, fiber-shaped PSCs with higher flexibility are more compatible with wearable electronics, electric-generating tents and other intelligent electric devices.

Some other novel flexible substrates have been investigated in PSCs [43–45]. For example, Ou et al. [43] introduced a shape-memory Noland Optical Adhesive 63 as flexible substrate in PSC. The flexible device can redeem to the initial shape through thermal annealing. See the images shown in Fig. 5(d). Interestingly, after 50 cycles of full crumpling, the device can still maintain 60% of its initial PCE.

4. Development of conductive and transparent electrodes

4.1. Conductive and transparent photoanodes for flexible PSCs

Indium tin oxide (ITO) was the most frequently used photoanode material, because high quality ITO films with high conductivity and transparency could be easily achieved on both rigid glass and flexible plastic substrates. The sheet resistant of ITO/plastic substrate is about 10–15 Ω/sq close to that of ITO/glass (7–15 Ω/sq) [39]. The optical transmittance of ITO/plastic substrate can reach 80% in the visible range [47]. However, some drawbacks of ITO material and its coating on flexible substrates cannot be ignored. First, indium element in ITO is rare and expensive metal [48]. Second, ITO coating is brittle and cannot bear high-curvature bending [49]. For example, Zardetto et al. [37] reported the degradation process of ITO/PET and ITO/PEN after bending with a radius of curvature from 16 mm to 2 mm. As shown in Fig. 6(a) and (b), when the radius decreases below 14 mm, the sheet resistances of the films get to increase, indicating that the films have been damaged. Therefore, it is important to explore alternative photoanode materials for flexible PSCs applications. In Table 2, there is a summary on the performance of flexible PSCs based on photoanode materials alternative to ITO. And the device configurations, notable points of

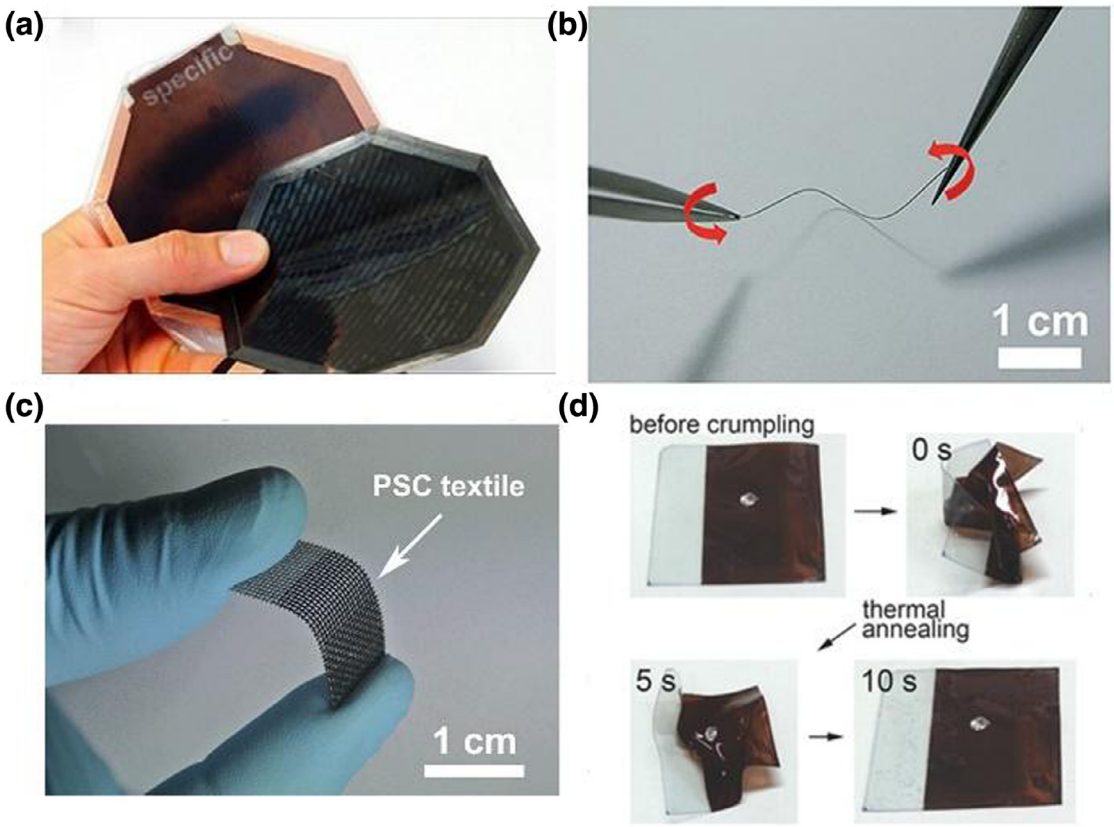

Fig. 5. (a) Photo of flexible PSCs based on a metal substrate [46]. Reproduction from ref. [46] with the permission from American Chemical Society; (b) photo of a perovskite fiber under twisting (c) photo of a piece of PSC textile [42]. Reproduction from ref. [42] with the permission from Royal Society of Chemistry; (d) recovering of crumped Noland Optical Adhesive 63 through heating at 80 °C for 10 s [43]. Reproduction from ref. [43] with the permission from Wiley.

key improvements, and performance characteristics are shown in this table.

PEDOT: PSS, a conductive polymer, has been demonstrated as a good candidate to replace ITO in flexible PSCs. It is reported they have a high conductivity up to 1400 S/cm [50], favorable solubility in water, and facile solution deposition with no need of high temperature treatment. Based on dimethylsulfoxide modified PEDOT: PSS as the photoanode material, Martin et al. [22] fabricated an ultrathin flexible PSC with the total thickness of 3 μm as shown in Fig. 6(c), which yielded an efficiency of 12.5%. Impressively, under 44% areal compression, the device can still maintain its initial photovoltaic performance.

Ag mesh is another promising electrode material to replace ITO for flexible PSCs. Li et al. [51] embedded hexagonal patterned Ag meshes into ultraviolet-resin-coated PET substrate, and spin-coated a PH1000 layer on it to prepare a hybrid photoanode, as shown in Fig. 6(d). The transmittance of the electrode is between 82% and 86%, and the sheet resistance is as low as 3 Ω/sq. The reported efficiency of the corresponding flexible PSC is up to 14%. It is noteworthy that, the initial efficiency decreases only 5% after 5000 bending cycles at the radius of 5 mm. This proves that the device with the hybrid photoanode has much better bendability than conventional ITO.

Due to the favorable conductivity and mechanical flexibility, carbon nanotubes (CNTs) and graphene have also been used as photoanodes in flexible PSCs. Matsuo et al. [52] deposited HNO_3 modified CNTs as the photoanode on PET substrate, achieving a sheet resistance of 85 Ω/sq and transmittance of above 90% in the visible range. The flexible PSC obtained an efficiency of 5.38%. Yan and co-workers [53] introduced graphene as the photoanode material on PET substrate and achieved an efficiency of 11.5%. Yoon et al. [10] later demonstrated a graphene photoanode based flexible PSC with a much higher efficiency of 16.8%. The device structure is shown in Fig. 7(a). A 2 nm-thick MoO_3 was covered on graphene to improve band alignment with respect to perovskite and overcome the hydrophobicity of graphene, facilitating deposition of the next PEDOT:PSS layer. Fig. 7(b), (c) and (d) show the higher transmittance and flexibility of graphene than that of ITO. In extreme conditions, the graphene based devices can retain 85% of the efficiency after 5000 bending cycles at a radius of 2 mm.

4.2. Conductive and transparent counter electrodes for flexible PSCs based on metal substrates

For metal substrates based PSCs, due to the opaque property of metals, transparent counter electrode is required for light entrance. Based on titanium (Ti) foil substrate, Wang et al. [54] firstly employed electrochemical anodization method to prepare TiO_2 nanotube arrays as counter electron transport interfacial layer; after deposition of perovskite and spiro-OMeTAD, they introduced a film made of carbon nanotubes as the counter electrode. The carbon nanotubes counter electrode had a transmittance between 60% and 80%. The flexible PSC finally achieved an efficiency of 8.31%. Ultrathin metal film has also been demonstrated as the counter electrodes in flexible PSCs. The optical transmittance and electric conductivity of the metal films are both sensitive to the film thickness [55]. A trade-off between transmittance and conductivity is normally required for the optimization of device. Lee et al. [56] employed a 12 nm-thick Ag film as the counter electrode in flexible PSC, resulting in an efficiency of 6.15%. At the meantime, the initial efficiency maintained over 98% after 100 cycles at a bending radius

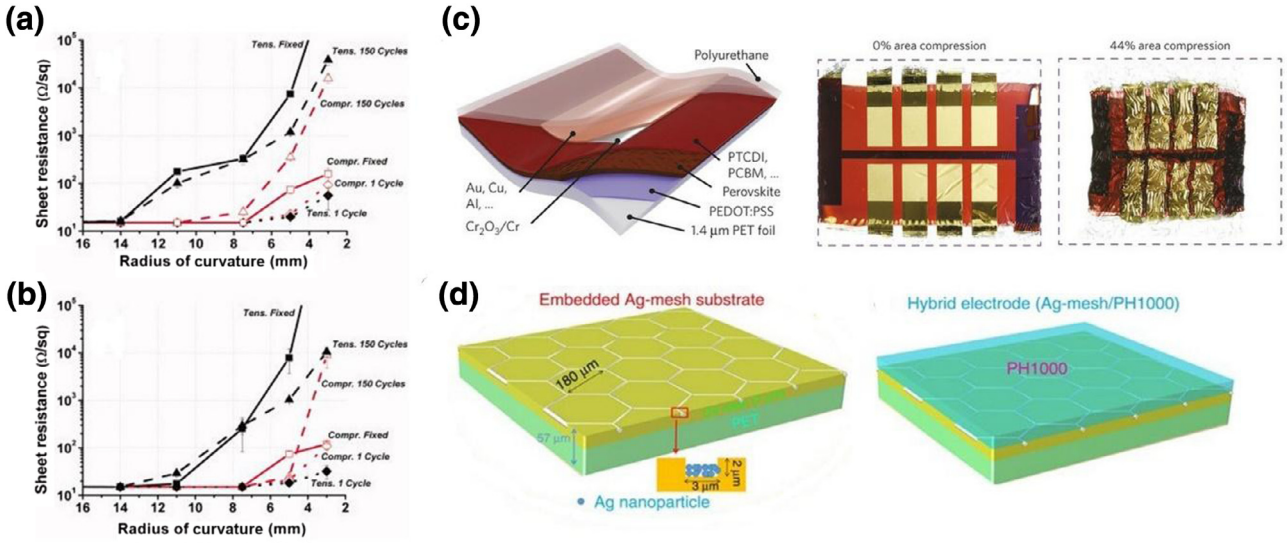

Fig. 6. (a) and (b) show the flexibility test results for PET/ITO and PEN/ITO substrates, respectively. Colors red and black present tensile and compressive stress, respectively. There are three conditions: fixed on a curved surface (squares-line), after 150 cycles (triangles-dashed) and after 1 cycle (diamonds-dotted) [37]. Reproduction from ref. [37] with the permission from Wiley; (c) schematic diagram of ITO-free flexible PSC based on PEDOT:PSS photoanode (left) and two photographs of the ultra-thin device before (middle) and after compression (right) [22]. Reproduction from ref. [22] with the permission from Nature Publishing Group; (d) schematic diagram of the hybrid photoanode (PET/Ag-mesh/PH1000) [51]. Reproduction from ref. [51] with the permission from Royal Society of Chemistry.

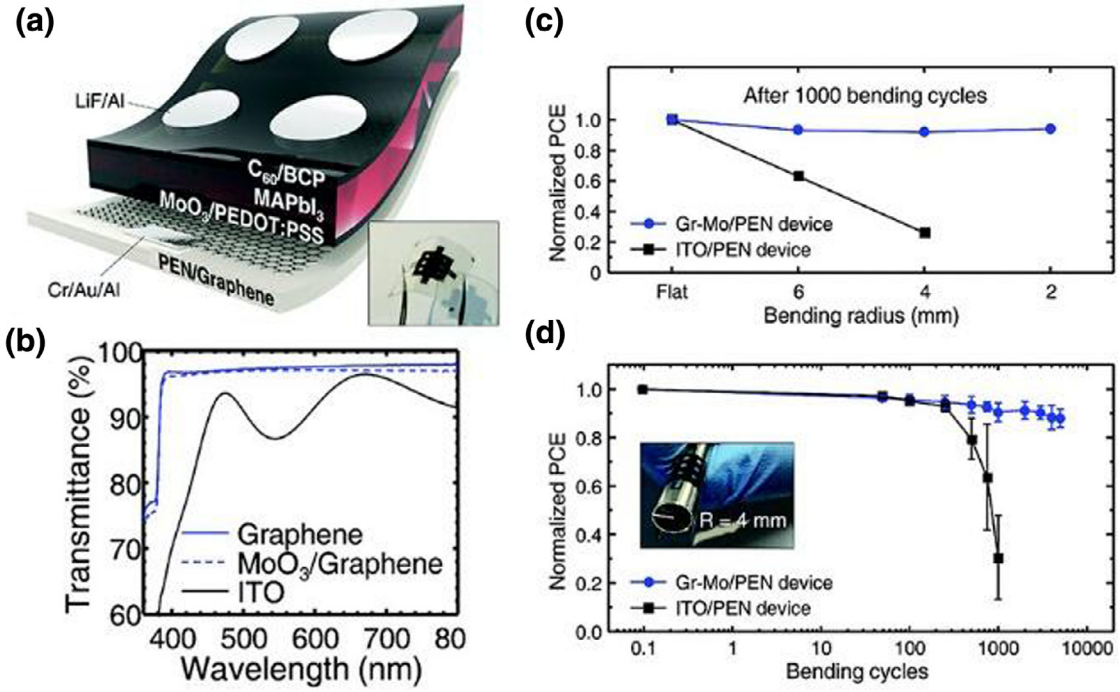

Fig. 7. (a) Device structure of the best performing flexible PSC; (b) transmittance of the ITO/PEN, Graphene/PEN, and Graphene-MoO_3/PEN substrates; (c) 1000 cycles' bending stability test of Graphene-MoO_3/PEN and ITO/PEN devices at radius of ∞, 6, 4, and 2 mm; (d) 10,000 cycles' bending test of Graphene-MoO_3/PEN and ITO/PEN devices at radius of 4 mm [10]. Reproduction from ref. [10] with the permission from Royal Society of Chemistry.

of 6 mm. Their group later embedded a 1 nm-thick Ag layer into ITO film and got highly transparent hybrid counter electrode. Their flexible PSC got an improved efficiency of 11.01% [57]. However, ultrathin metal films might be not continuous and dense; the poor conductivity normally becomes a limiting factor. In view of this, the combination of metal mesh and conductive polymer provide a solution to design a hybrid counter electrode. Troughton et al. [58] proposed a self-adhesive layer with Ni mesh embedding into PET which was then covered by a hybrid film of PEDOT and adhesive (Fig. 8a). Their flexible PSC achieved an efficiency of 10.3%, due to good contact between the electrodes and the hole transport interfacial layers. Nejand et al. [40] use a 150 nm-diameter Ag mesh through spray deposition as the counter electrode and Cu foil as the substrate (Fig. 8b). With CuI and ZnO as the p-type and n-type charge transport layers, the flexible PSC finally achieved an encouraging efficiency of 12.8%. In Table 3, there is a summary on the performance of flexible PSCs based on transparent and conductive counter electrodes. And the device configurations, notable points

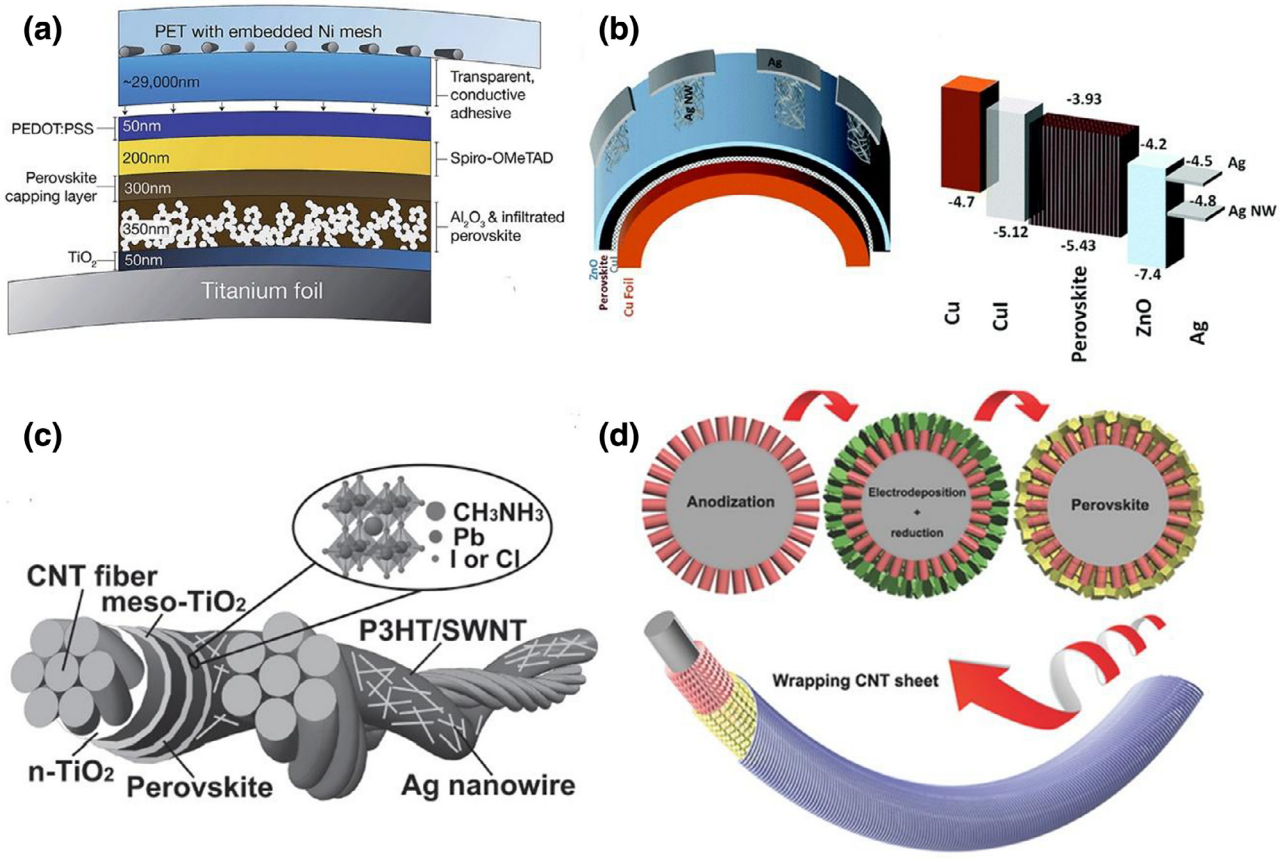

Fig. 8. (a) A Ti foil substrate based flexible PSC with a hybrid counter electrode [58]. Reproduction from ref. [58] with the permission from Royal Society of Chemistry; (b) schematic diagram of a Cu foil based flexible PSC and its energy level alignment [40]. Reproduction from ref. [40] with the permission from Royal Society of Chemistry; (c) schematic diagram of a double-twisted fiber PSC with carbon nanotubes [59]. Reproduction from ref. [59] with the permission from John Wiley and Sons; (d) schematic diagram shows the deposition process of perovskite layer on a Ti fiber and the device structure of the fibrous PSC [60]. Reproduction from ref. [60] with the permission from John Wiley and Sons.

of key improvements, and performance characteristics are shown in this table.

Recently, the fiber-shaped flexible PSCs have been successfully demonstrated [41,42]. Li et al. [59] proposed a double-twisted fiber-shaped PSC, which employed carbon nanotubes as the photoanode as well as the counter electrode. Combined with an outer layer made of Ag nanowires to promote charge transport, the best device yielded an efficiency of 3.03%. The device structure is shown in Fig. 8(c). This kind of device shows a rather good flexibility, maintaining almost 100% of the initial efficiency after 1000 times bending. Qiu et al. [60] later used cathodic deposition process to prepare perovskite layer with high coverage and uniformity on the fibrous Ti substrate (Fig. 8d), leading to a much higher efficiency of 7.1%. At the meantime, the efficiency can be maintained over 90% after 400 times bending. In Table 4, a summary on the performance of fibrous flexible PSCs is provided. The device configurations, notable points of key improvements, and performance characteristics are shown in this table.

5. Progress on the interfacial materials

As the indispensable parts of PSCs, interfacial layers undertake the function of extracting photo-generated carriers from perovskites to the electrodes. To avoid the charge accumulation, the efficient charge separation and the transport at the interfaces are important for efficiency and stability of the devices. Since 2015, the number of reports on low-temperature processed interfacial materials in PSCs has largely increased. Tables 5 and 6 show the performance of flexible PSCs based on different interfacial materials with regular and inverted configurations, respectively.

5.1. N-type electron transport interfacial materials

In PSCs, n-type interfacial layer is used for extracting photo-generated electrons and blocking holes to the counter electrode. This normally requires the n-type interfacial layers have suitable electronic affinity, high electron mobility and well-aligned energy levels with perovskites. Especially as a window layer in regular structured device, high optical transmittance of n-type interfacial layer is required for light entrance.

5.1.1. TiO_2

TiO_2 is the most frequently used n-type interfacial material in regular PSCs, which was initially used in dye-sensitized solar cells. Its conduction band edge (−4.1 eV versus vacuum) [79] is a little bit lower than the conduction band level of $MAPbI_3$ (−3.9 eV), facilitating the interfacial electron injection. In addition, its large bandgap of over 3.0 eV can prevent the hole injection from $CH_3NH_3PbI_3$ to its valance band [80]. Thus, it is efficient for electron selective extraction. In regular PSCs, a TiO_2 porous scaffold layer, on top of the TiO_2 compact layer, was required to improve electron extraction and alleviate hysteresis effect through reducing the diffusion length of electrons. However, the preparation of those TiO_2 compact layer and porous scaffold layer both required high

Table 2. Summary of the performance of ITO-free flexible PSCs.

Device configurations	Key improvements	V_{oc} (V)	J_{sc} (mA/cm^2)	FF (%)	Efficiency (%)	Ref.
PET/PEDOT:PSS/$CH_3NH_3PbI_3$/PCBM/Al		0.80	15.0	60.0	7.60	[61]
PET/MSA-PEDOT:PSS/$CH_3NH_3PbI_3$/PCBM/ rhodamine 101/C60/rhodamine 101/LiF/Ag		0.87	17.2	57.0	8.60	[62]
PET/PEDOT:PSS/$CH_3NH_3PbI_3$/PCBM/TiO_2/Al	Spray coated of PEDOT:PSS	0.75	15.8	41.0	4.90	[63]
PET/PEDOT:PSS/PEI/$CH_3NH_3PbI_3$/Spiro-MeOTAD/Au	PEI-modificated PEDOT:PSS	0.95	17.2	59.7	9.73	[51]
PET/AZO/Ag/AZO/PEDOT:PSS/Poly-TPD/$CH_3NH_3PbI_3$/PCBM/AU		1.04	14.3	47.0	7.00	[64]
PET/SWCNT/ $CH_3NH_3PbI_3$/PCBM/Al	HNO_3 doped SWCNT	0.71	11.8	56.0	5.38	[65]
PET/Ag-mesh/PH1000/PEDOT:PSS/$CH_3NH_3PbI_3$/PCBM/Al	Ultralight (1.96 W/g)	0.91	19.5	80.0	14.00	[52]
PET/Ag nano-network/graphene oxide/PEDOT:PSS/$CH_3NH_3I_3$/PFN-P1/PCBM/Ag		0.94	12.7	66.2	7.92	[66]
PES/PSSNa/Ag/PEI/PC61BM/$CH_3NH_3PbI_{3-x}Cl_x$/Spiro-MeOTAD/hc-PEDOT:PSS	PCBM doped by SDBAC	1.07	15.8	70.0	11.80	[67]
PET/graphene/P3HT/ $CH_3NH_3PbI_3$/PC_{71}BM/Ag	Ultralight (5.07 W/g); CVD deposited graphene	1.04	18.6	59.4	11.48	[53]
PEN/Graphene-Mo/PEDOT:PSS/$CH_3NH_3I_3$/C60/BCP/LiF/Al	CVD deposited graphene	1.00	21.7	0.8	16.80	[10]
PET/AZO/ZnO/C60/ $CH_3NH_3PbI_3$/Spiro-MeOTAD/MoO_3/ In_2O_3:H embedded with Ni/Al grid	RF sputtered AZO; thermally evaporated C_{60} and MoO_3	1.08	16.1	68.6	12.20	[68]
PET/IZO/TiO_2/$CH_3NH_3PbI_3$/Spiro-MeOTAD/Ag	Spin-coated TiO_2 nanoink	1.05	18.2	70.0	13.20	[69]
NOA 63/PEDOT:PSS/$CH_3NH_3PbI_3$/PCBM/Eutectic Ga–In blend	Shape recoverable cell	0.92	16.6	70.5	10.75	[43]
SU-8/MoO_3/Au/ PEDOT:PSS/$CH_3CH_3PbI_{3-x}Cl_x$/PCBM/Ca/Ag		0.93	13.2	73.9	9.05	[70]
NOA63/MoO_3/Au/PEDOT:PSS/$CH_3NH_3PbI_{3-x}Cl_x$/PCBM/DMD (MoO_3/Au/Ag/MoO_3/Alq3)	Semitransparent; ultrathin metallic electrodes	0.83	13.9	60.7	6.96	[71]
PET/IZO/TiO_2/$CH_3NH_3PbI_3$/Spiro-MeOTAD/Ag	Spin-coated TiO_2 nanoink	1.05	18.2	70.0	13.20	[69]

Table 3. Summary of flexible PSCs based on metal substrates.

Device configurations	Key improvements	V_{oc} (V)	J_{sc} (mA/cm^2)	FF (%)	Efficiency (%)	Ref.
Ti/c-TiO_2/mp-TiO_2/$CH_3NH_3PbI_3$/Spiro-MeOTAD/ultra-thin Ag	Electropolished Ti foil; $TiCl_4$ treated TiO_2 nanotubes	0.89	9.5	72.8	6.15	[56]
Ti/TiO_2 nanotubes/$CH_3NH_3PbI_3$/Spiro-MeOTAD/CNT	$TiCl_4$ treated TiO_2 nanotubes	0.99	14.4	68.0	8.31	[54]
Ti-foil/c-TiO_2/mp-Al_2O_3/$CH_3NH_3PbI_{3-x}Cl_x$/Spiro-MeOTAD/ PEDOT: PSS/PET with Ni mesh	Transparent conductive and adhesive counter electrode	0.98	17.0	61.0	10.30	[58]
Ti/c-TiO_2/mp-TiO_2/$CH_3NH_3PbI_3$/Spiro-MeOTAD/ITO	Sputtered ITO with ultra-thin Ag layer embedded as counter electrode	0.10	18.5	61.0	11.01	[57]
Ti/TiO_2/$CH_3NH_3PbI_3$/Spiro-MeOTAD/Ag nanowires	Spray coated Ag nanowires	0.92	16.5	49.0	7.45	[72]
Ti/ TiO_2 nanowire/$CH_3NH_3PbI_3$/PEDOT/PEN-ITO	Spin-coated TiO_2 nanowire array prepared through hydrothermal method; Electrodeposited PEDOT	0.94	21.7	63.0	13.07 (1 cm^2)	[73]
Cu/CuI/$CH_3NH_3PbI_3$/ZnO/Ag nanowires	Spray coated Ag nanowires	0.96	22.5	59.2	12.80	[40]

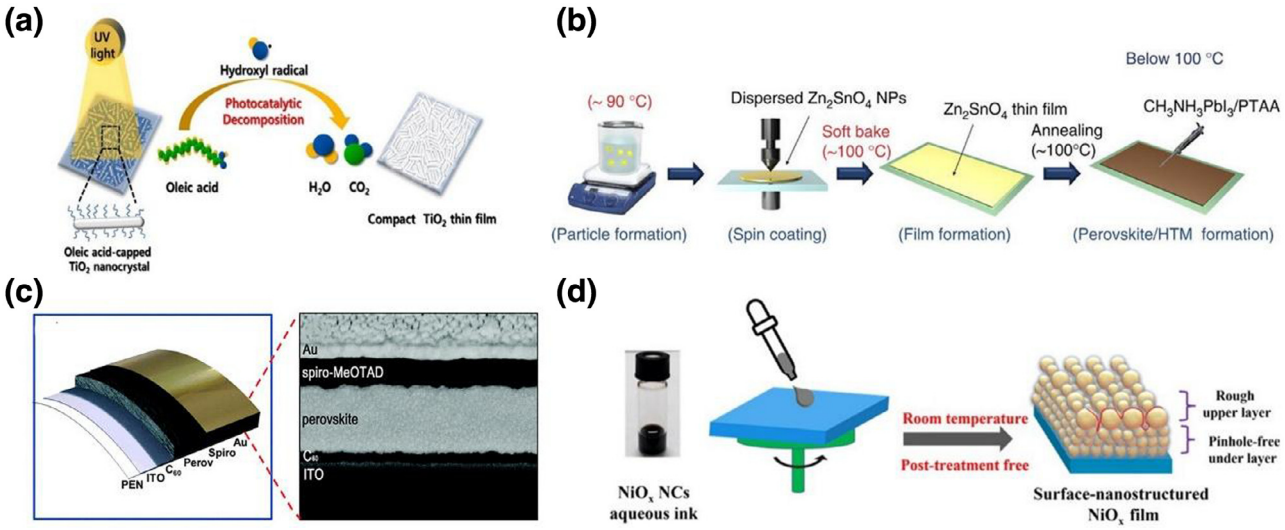

Fig. 9. (a) UV-assisted solution process for the preparation of compact TiO_2 thin film [85]. Reproduction from ref. [85] with the permission from Elsevier; (b) schematic illustration of the fabrication procedures of Zn_2SnO_4 based PSC [98]. Reproduction from ref. [98] with the permission from Nature Publishing Group; The device configuration (c) and cross-sectional SEM image (d) of a regular PSC with evaporated C60 as electron transport layer [110]. Reproduction from ref. [110] with the permission from Royal Society of Chemistry; (e) schematic illustration of the fabrication of NiO_x nanocrystalline film [129]. Reproduction from ref. [129] with the permission from American Chemical Society.

temperature treatment at ~500 °C. No plastic substrates can sustain such high temperature processing. Therefore, for flexible PSCs application, the key issue is to develop low-temperature techniques to prepare TiO_2 layers with high quality.

Kim et al. [49] employed atomic layer deposition technique to prepare TiO_2 compact layer with the thickness of 20 nm on PET/ITO substrate at 80 °C. Based on this n-type interfacial layer, their flexible PSC with the configuration of "PET/ITO/TiO_2/$CH_3NH_3PbI_{(3-x)}Cl_x$/Spiro-MeOTAD/Ag" has achieved an efficiency of 12.2%. Giacomo et al. [81] printed a porous TiO_2 layer on the atomic layer deposited TiO_2 compact layer, and treated it under UV-ozone to remove the organic component. The device gave an efficiency of 8.4%. Qiu et al. [82] prepared TiO_2 layer *via* e-beam induced evaporation and obtained an efficiency of 13.5%. Yang et al. [83] applied magnetron sputtering to deposit TiO_2 layer and reported a flexible PSC with an efficiency of 15.07%. Soon afterward, Mali et al. [84] used the similar sputtering method to fabricate a flexible PSC with the configuration of "PET/ITO/TiO_2/$CH_3NH_3PbI_{3-x}Br_x$/PTAA/Au" and obtained an enhanced efficiency of 15.88%. Besides vapor deposition techniques, nanoink strategy is frequently reported to make charge transport interfacial layers. Jeong et al. [85] introduced an Nd-doped TiO_2 nanoink and deposited the compact layer *via* UV-assisted solution process below 50 °C (Fig. 9(a)). The doping induced conductivity improvement and conduction band shift led to enhancement of electron extraction at the interface. Their best device got the efficiency of 16.01%. In addition, Lin et al. [86] prepared the TiO_2 compact layer via electrodeposition and obtained the flexible PSC with the best efficiency of 15.76%.

Many other low-temperature processes have been reported to prepare TiO_2 on glass substrates. They are easily extended to prepare flexible PSCs. For example, Yella et al. [87] synthesized rutile TiO_2 nanoink and spin-coated on glass/FTO substrate; they got an efficiency of 13.7% of their rigid PSC. Very recently, Tan et al. [88] reported the low-temperature deposition of chlorine-modified TiO_2 nanocrystalline film on ITO/glass substrate, and achieved a certified efficiency as high as 20.1%. It is suggested that the chlorine passivation plays an important role to improve efficiency and remove hysteresis effect by eliminating deep trap states at the perovskite interface.

5.1.2. ZnO

In the research history of PSCs, ZnO was the first to be used as the n-type interfacial material alternative to TiO_2. This is because the high quality ZnO films can be easily deposited at low-temperature *via* diverse techniques, such as chemical bath deposition [89], nanoink method [90] and electrodeposition [91]. Its valence band is −4.2 eV versus vacuum, even a little deeper than that of TiO_2. Combined with its large bandgap of 3.3 eV [92], ZnO shows well-matched energy levels with respect to perovskites in PSCs. The reported conductivity of ZnO (0.0031 mS/cm) is dramatically higher than that of TiO_2 (0.00006 mS/cm), which should be another important advantage for flexible PSC application [93].

Kumar et al. [33] prepared ZnO compact layer through electrodeposition and ZnO nanorods through chemical bath deposition as electron transport interfacial layer. They achieved an efficiency of 2.64% for flexible PSCs. Liu and Kelly [94] used ZnO nanoink to prepare the nanocrystalline film at low temperature. Their flexible PSCs based on this ZnO electron transport interfacial layer achieved an improved efficiency of 10.2%. Later, Heo et al. [93] used a similar method to prepare ZnO-based flexible PSC and raised the efficiency up to 15.5%. You et al. [95] used NiO_x and ZnO nanoinks to prepare nanocrystalline films as the p-type and n-type interfacial layers and constructed an inverted PSC with the configuration of "ITO/NiO_x/$MAPbI_{3-x}Cl_x$/ZnO/Al". The device on ITO glass substrate yielded an efficiency of 14.6%. This kind of devices features with extremely low cost for mass production.

However, ZnO has an intrinsic drawback on poor chemical stability which will hinder the long-term stability of PSCs. Even a PCBM layer was inserted between perovskite layer and ZnO layer to physically separate them, the decomposition of perovskite [96] could still occur, leading to irreversible degradation of the interfacial property and the device performance.

5.1.3. Zn_2SnO_4

Ternary oxide Zn_2SnO_4 has been widely applied in photoelectric field due to the outstanding optical and electrical properties, as well as the good stability in ambient and acidic conditions. Its conduction band edge is −4.1 eV versus vacuum and the bandgap is as large as 3.8 eV [97]. A regular structured flexible PSC based on spin-coated Zn_2SnO_4 nanocrystalline film yielded an efficiency

Table 4. Summary of the performance of fibrous flexible PSCs.

Device configurations	Key improvements	V_{oc} (V)	J_{sc} (mA/cm^2)	FF (%)	Efficiency (%)	Ref.
Stainless steel/c-TiO_2/mp-TiO_2/$CH_3NH_3PbI_3$/Spiro-MeOTAD/CNT sheet		0.66	10.2	48.7	3.30	[41]
Stainless steel/ZnO seed/ZnO nanorod/$CH_3NH_3PbI_3$/Spiro-MeOTAD/CNT		-	-	-	3.80	[42]
CNT fiber/c-TiO_2/mp-TiO_2/$CH_3NH_3PbI_{3-x}Cl_x$/P_3HT/SWNT/Ag NW		0.62	8.8	56.4	3.03	[59]
Ti/dimple c-TiO_2/mp-TiO_2/$CH_3NH_3PbI_3$/Spiro-MeOTAD/Ag NW	Spray-deposited Ag NWs	0.73	12.0	44.0	3.85	[74]
Ti /TiO_2 nanotube/$CH_3NH_3PbI_{3-x}Cl_x$/Spiro-MeOTAD/CNT sheet		-	-	-	5.22	[75]
Ti/c-TiO_2/meso–TiO_2/$CH_3NH_3PbI_{3-x}Cl_x$/Spiro-MeOTAD/Au	Magnetron sputtered Au electrode	0.71	12.3	60.9	5.35	[76]
Ti/c-TiO_2/meso–TiO_2/$CH_3NH_3PbI_3$/CNT	Cathodic deposited perovskite layer	0.85	14.5	56.0	7.10	[60]
PEN/ITO/TiO_2/$CH_3NH_3PbI_3$/CNT	Strip-shaped substrate; Chemical vapor deposited CNTs	0.91	15.9	65.6	9.49	[77]
Ti/TiO_2 nanotube/$CH_3NH_3PbI_3$/CNT		0.92	2.6	48.0	1.16	[78]

of 15.3% [98] (Fig. 9b). It is reported that the as-prepared Zn_2SnO_4 nanocrystalline film has higher optical transmittance than that of conventional TiO_2 compact film in the visible range. This group later used the bilayer of Zn_2SnO_4 nanoparticles (average size ~ 19.2 nm) and Zn_2SnO_4 quantum dots (average size ~ 5.7 nm) for efficient electron extraction and recombination suppression. They finally raised the device efficiency up to 16.5%, which is the highest for Zn_2SnO_4 based PSCs [35].

5.1.4. Fullerene derivatives

A well-studied fullerene derivative in OPVs, PCBM, with favorable solubility and high electron mobility, has also been sufficiently demonstrated as an efficient electron transport interfacial material in PSCs. The HOMO and LUMO levels are −6.0 eV and −4.2 eV versus vacuum, respectively [99]. It has been reported with higher electron extraction capability than conventional TiO_2 [100].

In inverted structured PSCs, through spin-coating on top of perovskite, PCBM can permeate into the grain boundaries of perovskites and passive the interfacial defects to get the optimized device performance [101]. Typically, an additional buffer layer is required to insert between the PCBM layer and metal counter electrode to promote the Ohmic contact [102] For example, BCP [103], some metal oxides like TiO_x [36] and ZnO [104] have been used.

Recently, there are also some reports introducing PCBM into regular structured PSCs. Ryu et al. [105] employed TiO_2/PCBM bilayer electron transport interfacial material in regular PSC, giving an efficiency of 11.1%. Qin et al. [67] reported that stearyldimethylbenzylammonium chloride (SDBAC) doped PCBM could get higher conductivity and overcome the hydrophobicity of PCBM, benefiting to easier deposition of perovskite layer on it. Flexible PSC with the configuration of "PES/PSSNa/Ag grid/SDBAC-doped PCBM/$CH_3NH_3PbI_{3-x}Cl_x$/Spiro-MeOTAD/PEDOT: PSS" finally achieved an efficiency of 11.8%. C_{60} with a HOMO level of − 6.2 eV and a LUMO level of − 4.5 eV versus vacuum [106] was reported to be superior in term of electron mobility (C_{60} ~ 1.6 cm^2/ V·s versus PCBM ~ 6.1×10^{-2} cm^2/V·s) and conductivity (C_{60} ~ 2.3×10^{-3} S/cm versus PCBM ~ 3.2×10^{-4} S/cm) [107]. However, the solubility of C_{60} is much lower than that of PCBM [108], therefore, C_{60} layer is usually deposited by thermal evaporation [109]. Yoon et al. [110] introduced thermal-evaporated C_{60} into the regular structured PSC as electron transport interfacial layer and controlled the thickness of 35 nm; the device yielded a high efficiency of 16.0% on flexible substrate, and 19.1% on conductive glass substrate. The device structure is shown in Fig. 9(c).

5.1.5. Others

In addition to the above-mentioned materials, other metal oxides like W(Nb)O_x [111], Nb_2O_5 [112], SnO_2 [113] and some organic materials such as solid-state ionic-liquids (ss-IL) [35], N,N¢′-*bis*(3-(dimethylamino)propyl)−5,11-dioctylcoronene-2,3,8,9-tetracarboxdiimide (CDIN) [114] have also been used as n-type interfacial materials in flexible PSCs. Among them, one of the highest efficiencies (16.09%) was achieved by incorporating 1-benzyl-3-methylimidazolium chloride, one kind of ss-IL, as the electron transport interfacial layer [35]. The enhanced efficiency was attributed to downshift work function of ITO after ss-IL modification, from 4.67 eV to 4.32 eV, and high electron mobility of ss-IL [115].

Actually, more interfacial materials were deposited at low temperature in ITO glass and the corresponding rigid PSCs got much higher performances. For example, You and co-workers [116] reported a low-temperature deposited SnO_2 nanocrystalline film and achieved a certified efficiency of 19.9% for a regular structured PSC. It can be expected that similarly high efficiencies can be almost maintained when the rigid ITO glass is replaced by the flexible substrates since the low-temperature processes don't need to change.

5.2. P-type hole transport interfacial materials

2,2′,7,7′-Tetrakis-(N,N-di-4-methoxyphenylamino)−9,9′-spirobifluorene (spiro-MeOTAD), Poly[*bis*(4-phenyl)(2,5,6-trimethylphenyl)amine (PTAA) and PEDOT: PSS are p-type interfacial materials used the most frequently, owing to their simple film fabrication at low temperature, well-matched energy levels for perovskites and acceptable electric conductivities [117]. However, there are still some open questions for these materials which cannot be ignored. For example, when spiro-MeOTAD and PTAA were used as hole transport interfacial materials, some extra additives like *bis*(trifluoromethanesulfonyl)imide (TFSI) and *tert*-butylpyridine (*t*BP) are required to enhance conductivity and achieve higher performance [118,119]. These additives would also induce some stability issues. For example, *t*BP can induce the corrosion of the perovskite [120], and moisture sensitive TFSI can diffuse into perovskite under bias [121]. The high acidity of PEDOT:PSS (PH = 1) has a high risk to corrode the ITO electrode [122]. The moisture sensitive PEDOT:PSS normally shows a poor stability in ambient condition [123].

NiO is an intrinsic p-type semiconductor with good chemical stability and wide bandgap (3.6 eV) [124]. Its conduction band

Table 5. Summary of the performance of flexible PSCs with regular structures on ITO coated flexible substrates.

Device configurations	Key improvements	V_{oc} (V)	J_{sc} (mA/cm^2)	FF (%)	Efficiency (%)	Ref.
TiO_2 as N-type interfacial material						
PEN/ITO/TiO_x/$CH_3NH_3PbI_{3-x}Cl_x$/Spiro-MeOTAD/Ag	ALD deposited TiO_2	0.95	21.4	60.0	12.20	[49]
PET/ITO/c-TiO_2/mp-TiO_2/$CH_3NH_3PbI_{3-x}Cl_x$/Spiro-MeOTAD/Au	ALD deposited TiO_2 compact layer;	0.86	14.1	70.0	Cell~8.40 (0.12 cm^2)	
	UV irradiated mesoporous TiO_2	3.39	5.2	71.0	Module~3.10(7.92 cm^2)	[81]
PET/ITO/TiO_2/$CH_3NH_3PbI_3-_xCl_x$/Spiro-MeOTAD/Ag	Ultrasonic spray-coated perovskite and photonic cured TiO_2	1.03	15.3	51.4	8.10	[136]
PET/ITO/TiO_2/$CH_3NH_3PbI_{3-x}Cl_x$/PTAA/Au	Electron beam evaporated TiO_2	0.91	21.3	69.0	13.50	[82]
PET/ITO/TiO_2/CH_3NH_3Pb $I_{3-x}Cl_x$ /Spiro-MeOTAD /Au	Sputtered TiO_2	1.03	20.9	70.0	15.07	[83]
PET/ITO/SnO_x/BK-TiO_2/$CH_3NH_3PbI_{3-x}Cl_x$/Spiro-MeOTAD/Au		1.03	~19.0	~68.0	13.40	[89]
PEN/ITO/UV-Nb:TiO_2/$CH_3NH_3PbI_3$/Spiro-MeOTAD/Au	UV-assisted solution process prepared Nd-doped TiO_2	1.04	20.2	76.0	16.01	[85]
PET/ITO/c-TiO_2/mp-TiO_2/$CH_3NH_3PbI_3$/Spiro-MeOTAD/Au	Plasma-assisted ALD deposited TiO_2 compact layers	0.88	14.9	70.0	9.20	[137]
PET/ITO/TiO_2/ CH_3NH_3Pb $(I_{1-x}Br_x)_3$/PTAA/Au	RF sputtered TiO_2	1.11	20.8	69.0	15.88	[84]
PEN/ITO/c-TiO_2/BK-TiO_2/ $CH_3NH_3PbI_3$/Spiro-MeOTAD/Au	Anodical electrodeposited compact layer TiO_2	1.07	19.5	75.0	15.76	[110]
PET/ITO/c-TiO_2/me-TiO_2/$CH_3NH_3PbI_{3-x}Cl_x$/Spiro-MeOTAD/Au	ALD deposited TiO_2 compact layer; UV irradiated mesoporous TiO_2	0.66	33.7	77.3	12.10 under LED illumination (400 lx ; MPD = 16.0 μW/cm^2)	[138]
ZnO as N-type interfacial material						
PET/ITO/c-ZnO/ZnO nanorod/$CH_3NH_3PbI_3$ Spiro-MeOTAD/Au	Electrodeposited ZnO compact layer; CBD grown ZnO nanorods	0.80	17.5	43.1	2.62	[34]
PET/ITO/ZnO/$CH_3NH_3PbI_3$/Spiro-MeOTAD/Ag	Spin-coated ZnO nanoparticles	1.03	13.4	73.9	10.20	[94]
PET/ITO/ZnO/$CH_3NH_3PbI_3$/C	Non-HTL; blade coated carbon paste	0.76	13.4	42.0	4.29	[139]
PET/ITO/graphite/ZnO-QDs/$CH_3NH_3PbI_3$/Spiro-MeOTAD/Ag	plasma jet (APjet)-treated ZnO quantum dots	0.94	16.8	62.0	9.73	[140]
PEN/ITO/ZnO/ $CH_3NH_3PbI_3$/PTAA/Au	Spin-coated ZnO nano-sol	1.10	18.7	76.0	15.50	[93]
PET/ITO/ZnO/$CH_3NH_3PbI_3$/Spiro-MeOTAD/Au	Sputtered ZnO	0.87	19.2	67.6	11.29	[141]
PI/ITO/ZnO/$CH_3NH_3PbI_3$/PTAA/Au	Roll-to-roll sputtered ITO	1.10	17.6	79.4	15.40	[38]
Flexible glass/ITO/ZnO/$CH_3NH_3PbI_3$/Spiro-MeOTAD/Au	PDMS anti-reflection layer; Sputtered ZnO	0.98	19.3	69.0	13.14	[44]
Zn_2SnO_4 as N-type interfacial material						
PET/ITO/$ZnSnO_4$/$CH_3NH_3PbI_3$/PTAA/Au	Spin-coated $ZnSnO_4$ nanoparticle	1.05	21.6	67.0	15.30	[98]
PEN/ITO/Zn_2SnO_4/$CH_3NH_3Pb(I_{0.9}Br_{0.1})_3$/PTAA/Au	Spin-coated Zn_2SnO_4 nanoparticles and quantum dots	1.10	20.4	73.0	16.50	[35]
PET/ITO/Zn_2SnO_4/PCBM/$CH_3NH_3PbI_3$/Spiro-MeOTAD/Ag	Spin-coated $ZnSnO_4$ nanoparticle prepared through hydrothermal method	1.05	17.4	63.8	11.61	[142]
Others						
PEN/FTO/TiO_2/PCBM/$CH_3NH_3PbI_3$/PTAA/Au		0.99	18.7	60.0	11.10	[105]
PET/ITO/ZnO/PCBM/ $CH_3NH_3PbI_3$/P3HTa/dry PEDOT:PSS/Ag	Fully slot-die cell except Ag electrode printed	0.84	11.4	56.0	5.40	[104]
PET/ITO/FPI-PEIE/PCBM/$CH_3NH_3PbI_3$/Spiro-MeOTAD/Au		1.07	17.8	53.0	10.00	[143]
PET-ITO/Ti/$CH_3NH_3PbI_3$/Spiro-MeOTAD/Ag	RF sputtered metallic Ti as electron transport interfacial layer	0.83	15.2	66.0	8.39	[144]
PET/ITO/ss-IL/$(HC(NH_2)_2PbI_3)_{0.85}(CH_3NH_3PbBr_3)_{0.15}$/Spiro-OmeTAD/Au	MgF_2 as an antireflection coating	1.07	22.7	66.2	16.09	[35]
PET/ITO/Al_2O_3/ $CH_3NH_3PbI_3$/Spiro-MeOTAD/Au	ALD deposited Al_2O_3	~1.00	~22.8	~67.0	14.60	[145]
PET/ITO/PEIE/CDIN/$CH_3NH_3PbI_3$/Spiro-MeOTAD/Ag		1.02	19.7	70.4	14.15	[114]
PEN/ITO/W(Nb)O_x/ $CH_3NH_3PbI_{3-x}Cl_x$/Spiro-MeOTAD/Ag	W(Nb)O_x Modified by Nb^{5+}	0.98	21.4	75.0	15.65	[111]
PET/ITO/Nb_2O_5/$(HC(NH_2)_2PbI_3)_{0.85}(CH_3NH_3PbBr_3)_{0.15}$/spiro-OMeTAD/Au	e-beam evaporated Nb_2O_5	1.12	23.5	63.1	15.56	[112]
PEN/ITO/PEIE/PCBM/ $CH_3NH_3PbI_3$/LN-P3HT/Au	Li doped P3HT	~0.88	~22.0	~69.6	13.12 (1 cm^2)	[133]
PEN/ITO/PEIE/PCBM/$CH_3NH_3PbI_3$/Co–P3HT/ Au	Co doped P3HT	1.01	19.8	59.3	11.84 (1.4 cm^2)	[132]
PET/ITO/Li:SnO_2/$CH_3NH_3PbI_3$/Spiro-MeOTAD/Au	Li doped SnO_2	1.02	20.6	76.3	14.78	[113]
PEN/ITO/SnO_2/PCBM/$CH_3NH_3PbI_3$/Spiro-MeOTAD/Au	PLD formed SnO_2	1.08	20.6	63.0	14.00	[146]
PEN/ITO/C_{60}/$CH_3NH_3PbI_3$/Spiro-MeOTAD/Au	Evaporated C_{60}	1.02	23.2	67.3	16.00	[110]
PEN/ITO/PEIE/C_{60}/$CH_3NH_3PbI_3$/Spiro-MeOTAD/Ag	Evaporated C_{60}	1.02	17.9	73.0	13.30	[147]
PET/ITO/$[HC(NH_2)_2PbI_3]_{0.9}[CH_3NH_3PbCl_3]_{0.1}$/Spiro-MeOTAD /Au		0.96	20.7	64.0	12.70	[148]
PEN/ITO/ $CH_3NH_3PbI_3$/Spiro-MeOTAD/MoO_3/Ag	One-step gas pump drying method prepared perovskite layer	0.96	17.4	56.0	11.34	[149]

(−1.8 eV) [125] and valence band (−5.33 eV) [126] match well with conventional perovskites. Many low temperature strategies were used to prepare NiO thin film on glass substrates such as pulsed laser deposition [127], magnetron sputtering [128] and nanoink strategies. For example, Zhang et al. [129] synthesized NiO_x nanocrystals through chemical precipitation method and got NiO_x aqueous nanoink as shown in Fig. 9(d). By spin-coating NiO_x nanocrystalline film on PET/ITO substrate, combined with PCBM/*Bis*-C60 as the electron transport interfacial layer, the inverted PSC gave an efficiency of 14.53%. Other reports about NiO based flexible PSCs also utilized similar nanoink route to prepare the NiO layers [25,130,131].

Besides, poly(3-hexylthiophene) (P3HT) [132,133], (1,4-*bis*(4-sulfonatobutoxy)benzene and thiophene moieties) (PhNa-1T) [134], and CuI [40] have been reported as alternative p-type hole transport interfacial materials in flexible PSCs. In rigid PSCs, low-temperature processed inorganic cupreous compounds recently got some evident progress. For example, a rigid PSC with the configuration of "FTO/TiO_x/$CH_3NH_3PbI_{3-x}Cl_x$/$CuGaO_2$/Au" with low-temperature deposited $CuGaO_2$ nanocrystalline film as hole transport interfacial layer, has achieved a remarkable efficiency of 18.51% [135].

6. Toward roll-to-roll fabrication of flexible PSCs

As an industrialized manufacturing technique with the benefit of high production rate, roll-to-roll (R2R) fabrication has been widely applied in diverse fields. At the beginning, it was widely used in conventional newspaper printing field. Now, it has been demonstrated as a cost effective way to realize mass production in photoelectric field which is compatible with plastic and metallic substrates. In addition, plenty of film deposition techniques can be integrated in the R2R production line, such as vacuum deposition (including thermal evaporation, magnetron sputtering, and chemical vapor deposition, etc.), gravure printing, slot-die coating, doctor blading, ink-jet printing, and laser ablation [156,159].

For laboratory research of PSCs, spin-coating is the most frequently used technique for thin films deposition. It is facile to fabricate small area thin films with controlled thickness and morphology, by simply controlling the rotatory speed, the time, as well as the concentration and the viscosity of the solution precursors. However, spin-coating is not suitable for large-area film fabrication. The reasons are as follows: first, a large portion of solution is wasted during spin-coating; second, different line speeds along the rotation center toward the side edges results in different centrifugal forces, which will lead to the uniformity problems of large-area films.

Blade-coating is another widely used film fabrication technique, which employs a blade with a certain gap with respect to the substrate to coat the film and scrap away the redundant solution precursor [160]. Yang et al. [33] used blade-coating to prepare all of the active layers in inverted structured PSCs, including PEDOT:PSS, perovskite, PCBM, on ITO/glass and ITO/PET substrates. After annealing each layers consecutively and evaporating Ag thin film as the counter electrode, the devices achieved an efficiency of 10.44% on ITO/glass substrate and 7.14% on ITO/PET substrate. Zhou et al. [139] blade-coated conductive carbon paste onto perovskite layer as the counter electrode, delivering an efficiency of 4.29% in a non-HTL structured PSC with the configuration of "PET/ITO/ZnO/$CH_3NH_3PbI_3$/Carbon". However, blade-coating is only suitable for low-volatile solutions with suitably high viscosities, because the solution precursor will quickly evaporate or flow away during coating. Besides, a certain portion of solution precursor will also be wasted during film coating, though less than spin-coating.

Slot-die coating is a promising technique for the scale-up film fabrication. It can be compatible with a broad range of inks with

Table 6. Summary of the performance of flexible PSCs with inverted structures on ITO coated flexible substrates.

Device configurations	Key improvements	V_{oc} (V)	J_{sc} (mA/cm^2)	FF (%)	Efficiency (%)	Ref.
PET/ITO/PEDOT:PSS/$CH_3NH_3PbI_{3-x}Cl_x$/PCBM/TiO_x/Al		0.88	14.4	51.0	6.40	[36]
PET/ITO/PEDOT:PSS/$CH_3NH_3PbI_3$/PCBM/Bis-C_{60}/Ag		0.86	14.6	75.0	9.43	[102]
PET/ITO/PEDOT:PSS/$CH_3NH_3PbI_{3-x}Cl_x$/PCBM/Bis-C_{60}/Al		0.86	16.5	64.0	9.20	[101]
PET/ITO/PEDOT:PSS/$CH_3NH_3PbI_3$/PCBM/BCP/Al		0.92	7.9	62.0	4.50	[103]
PET/ITO/PEDOT:PSS/$CH_3NH_3PbI_3$/PCBM/Ca/Al		0.99	17.2	72.0	12.25	[150]
PET/ITO/PEDOT:PSS/$CH_3NH_3PbI_3$/PCBM/Ca/Al		0.92	15.0	49.2	6.80	[151]
PET/ITO/PEDOT:PSS $CH_3NH_3PbI_3$/PCBM/Bis-C_{60}/Ag	Blade coated all active layers	0.87	13.9	59.0	7.14	[33]
PET/ITO/PEDOT:PSS/$CH_3NH_3PbI_{3-x}Cl_x$/PCBM/ZnO/Ag	Fully slot-die cell except Ag electrode printed	0.90	10.9	50.0	4.90	[104]
PET/ITO/PEDOT:PSS/C3-SAM/$CH_3NH_3PbI_{3-x}Cl_x$/PC_{61}BM/ZnO/Ag	Slot-die coated PEDOT: PSS and perovskite; Modified PEDOT: PSS	0.98	13.7	38.0	5.10 (0.5 cm^2)	[152]
PET/ITO/PEDOT:PSS/PEI-HI/ $CH_3NH_3PbI_{3-x}Cl_x$ /MAPbI$_3$/PCBM/LiF/Ag		19.01	1.1	68.0	13.80	[153]
PET/ITO/NiO_x/$CH_3NH_3PbI_3$/PCBM/Bis-C_{60}/Ag	Spin-coated NiO_x nanoparticle	1.00	20.7	70.5	14.53	[129]
PET/ITO/NiO_x/$CH_3NH_3PbI_3$/PCBM/Ag	Spin-coated NiO_x nanoparticle	1.04	18.7	68.9	13.43	[130]
PEN/ITO/NiO_x/$CH_3NH_3Pb(I_{0.9}Cl_{0.1})_3$/ PCBM/ BCP/Ag	Spin-coated NiO_x nanoparticle	1.04	17.7	64.2	11.84	[131]
PET/ITO/NiO_x/$CH_3NH_3PbI_3$/C_{60}/Bis-C_{60}/Ag	Spin-coated NiO_x nanoparticle	1.00	20.9	69.6	14.19	[29]
PEN/ITO/ PEDOT:PSS/ $CH_3NH_3PbI_3$/C_{60}/BCP/LiF/Al	Vacuum thermal evaporated C_{60}, BCP and LiF	0.97	21.5	83.0	17.30	[10]
PET/ITO/PEDOT:PSS/$CH_3NH_3PbI_3$/PCBM/Ag	Blading-coated perovskite layer	0.89	19.4	68.3	11.29	[154]
PEN/ITO/PEDOT:PSS/$FASnI_3$/C_{60}/BCP/Ag	Pb-free; evaporated BCP and C_{60}	0.31	16.1	62.6	3.12	[155]
PEN/ITO/PhNa-1T/$CH_3NH_3PbI_3$/PCBM/Ag		1.03	18.4	77.4	14.70	[134]
PET/ITO/$CH_3NH_3PbI_{3-x}Cl_x$/PCBM/Ag	Slot-die coated active layers	0.67	12.4	42.4	2.90	[157]
ITO/$CH_3NH_3PbI_3$/PCBM/Al		0.96	14.8	68.1	9.70	[158]
AgNW-GFRHybrimer/c-ITO/PEDOT:PSS/$CH_3NH_3PbI_3$/PCBM/BCP/Ag	Evaporated BCP	0.99	21.5	66.0	14.15	[45]

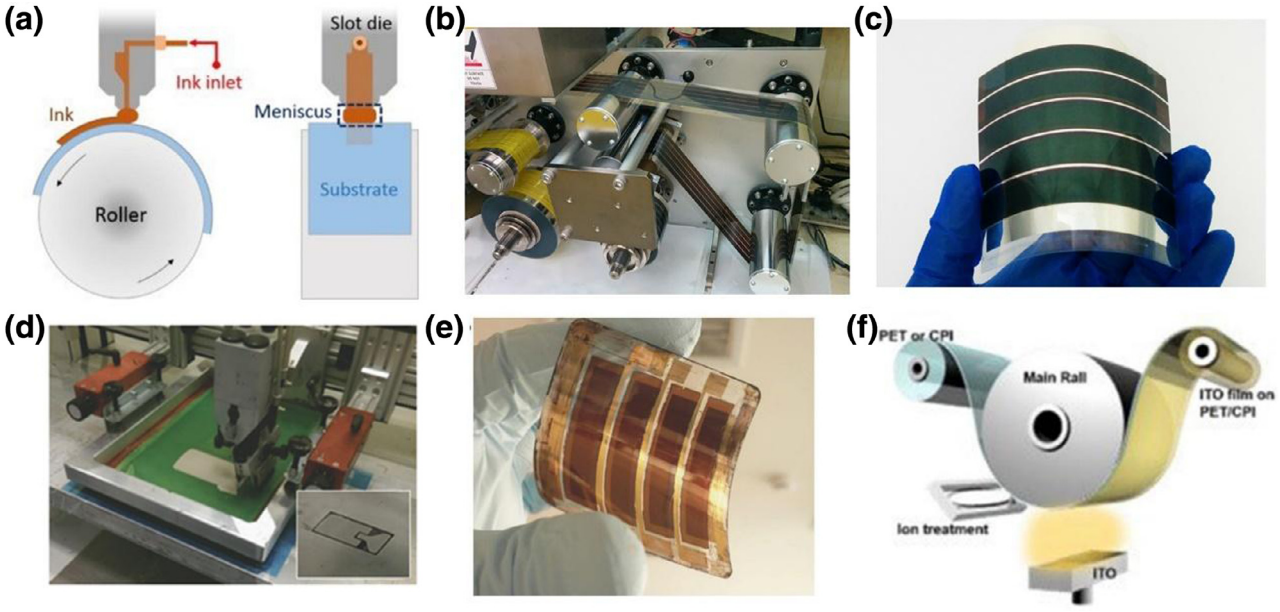

Fig. 10. (a) Mechanism of slot-die coating [157]. Reproduction from ref. [157] with the permission from Elsevier, (b) R2R slot-die coating of perovskite layer, (c) a photo of a flexible PSC module made of 5 cells (each with active area of 8 cm^2) in series connection [32]. Reproduction from ref. [32] with the permission from John Wiley and Sons, (d) a photo of screen printing of Ag counter electrode [104]. Reproduction from ref. [104] with the permission from John Wiley and Sons, (e) a photo of a module which has 4 cells (whole active area is 7.92 cm^2) in series connection [81]. Reproduction from ref. [81] with the permission from John Wiley and Sons. And (f) illustration of R2R sputtering deposition of ITO film on flexible substrate [38]. Reproduction from ref. [38] with the permission from Elsevier.

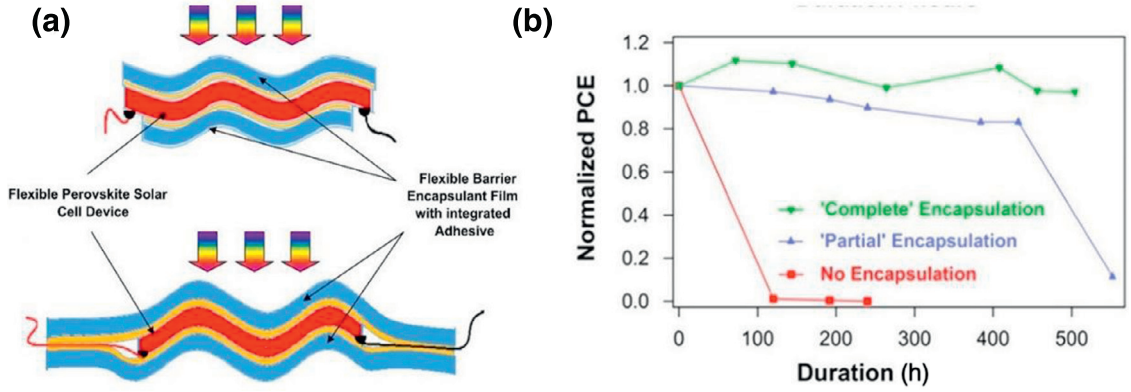

Fig. 11. (a) Schematic images show the partial encapsulation (top) and complete encapsulation (bottom) of flexible PSCs. (b) Normalized PCE of non-encapsulated, partially encapsulated, and completely encapsulated flexible PSCs as a function of storage time under ambient atmosphere [69]. Reproduction from ref. [69] with the permission from Elsevier.

different concentrations and viscosities, and the film thickness can also be controlled precisely [39]. The solution precursor is squeezed out through a slit with controlled gaps from the container by air pressure, and coated on a removable substrate. The working mechanism is schematically shown in Fig. 10(a). Slot-die coating uses a sealed container to keep the solution precursor, therefore, the solution condition can be kept constant during coating. Furthermore, not like spin-coating or blade-coating, the solution precursor for slot-die coating will not be wasted. Hwang et al. [32] firstly applied slot-die coating to prepare all of the active layers of the PSCs on ITO/glass substrate. Their small-area device finally obtained an efficiency of 11.96%. In the meantime, they have demonstrated a large-area flexible PSC module through the same fabrication procedures. The module with total active area of 40 cm^2 (Fig. 10c), finally achieved an efficiency of ~1%. Later, Schmidt et al. [104] employed slot-die coating to prepare all of the active layers in the flexible PSCs, with the Ag counter electrode deposited *via* screen printing (Fig. 10d). The efficiency has reached 5.4% and 4.9% in regular and inverted structured PSCs, respectively.

Besides, some scalable techniques, which could be integrated in R2R production line, have also been used to prepare one or a few active layers in flexible PSCs. For example, Giacomo et al. [81] used screen-printing to deposit TiO_2 scaffold layer on a ITO/PET flexible substrate. With the configuration of "PET/ITO/c-TiO_2/mp-TiO_2/$CH_3NH_3PbI_{3-x}Cl_x$/spiro-MeOTAD/Au", the flexible perovskite module achieved 3.1% efficiency (~32 cm^2) (Fig. 10e). In another example, R2R sputtering has been used to prepare ITO films on plastic flexible substrate (Fig. 10f) [38].

7. Encapsulation technologies for flexible PSCs

In the practical applications, robust stability and considerable lifetime are the critical standards to evaluate solar cells. However, when exposed to the ambient condition, organometal halides perovskite materials have a high risk to decompose, which would further corrode the metal counter electrode and damage the device structure. Moisture, oxygen, light (especially UV light), heat, electric bias and their combined impacts could accelerate the

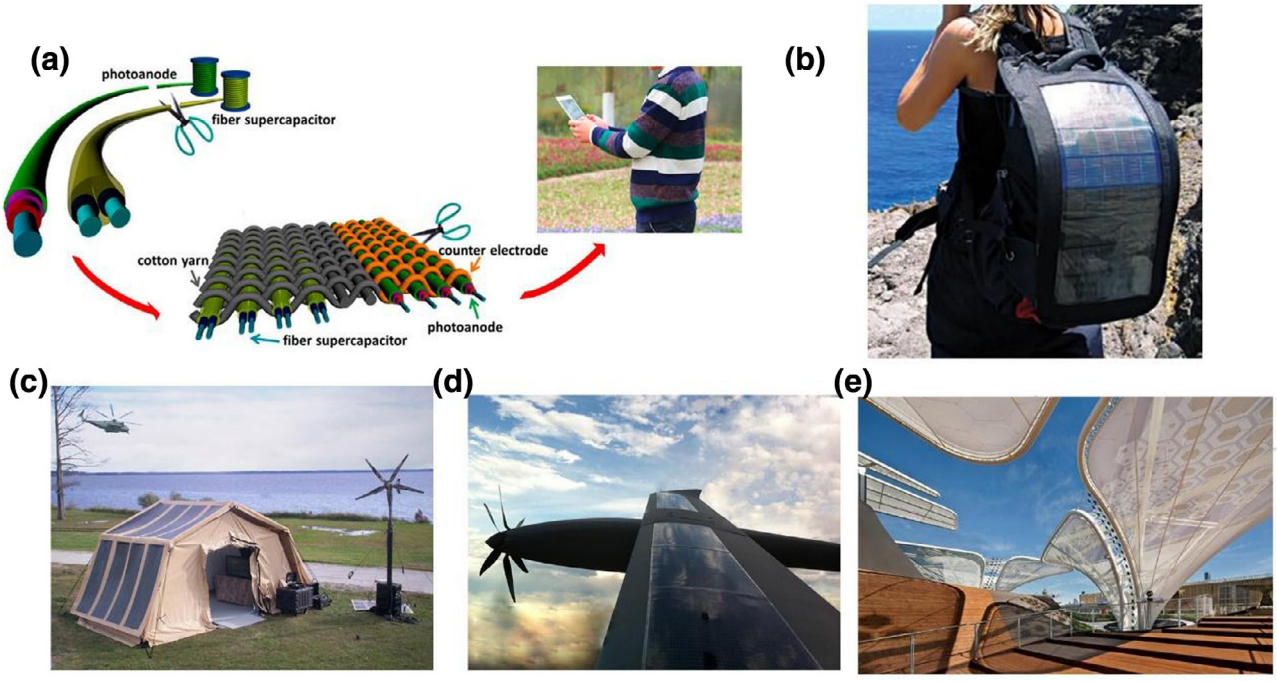

Fig. 12. (a) Schematic image shows the structure of future smart clothes integrated with fiber-shaped supercapacitors and dye-sensitized solar cells [168]. Reproduction from ref. [168] with the permission from American Chemical Society; (b) a bag covered by CIGS flexible solar panels [169]; (c) a photo of solar powered tents made by Energy Technologies Inc. [170], (d) a photo of solar powered unmanned aircraft system designed by Silent Falcon^{TM} UAS Technologies [171], (e) a photo of OPVIUS organic BIPV construction material from BELECTRIC [172].

decomposition rate. Some reports showed that if a $CH_3NH_3PbI_3$ based PSC is exposed in the atmosphere with the humidity of ~55%, the efficiency could decrease over 50% after just one day [161]; and if the humidity of the atmosphere is 95%, obvious degradation could be observed only after one hour [162]. In view of the critical stability issues of PSCs, encapsulation technology becomes an imperative part for its further industrialization.

For conventional encapsulation of rigid PSCs, a glass cover is normally used to seal the active layers. The edges of the cover glass were sealed with the substrate by UV-curable epoxy resin, and some drying agent was put inside the cavity between them to further absorb moisture [163]. Unfortunately, many encapsulation techniques used in rigid PSCs cannot be applied in flexible PSCs. It is required to develop alternative thin-film encapsulation technologies compatible for flexible substrates. Besides, for flexible PSCs, many of the substrates reported are plastic, which have much higher water vapor transmission rate (WVTR) (for example, ~18.13 g/(m^2•d) for PET at 37 °C and 90% relative humidity [164]) than the rigid glass. Therefore, flexible PSCs need additional water-resistant barriers to prevent water permeation from the plastic substrates. There are four key points for thin-film encapsulation technology: flexible property, low WVTR, easy formation onto the device without damage, and simple process with high efficiency.

PVD, PECVD, ALD, PEALD and other techniques have been used for thin film encapsulation. According to the film structure, it can be divided into two types, i.e., single-layer thin-film encapsulation and multilayer thin-film encapsulation. Single-layer thin-film encapsulation simply uses one inorganic film for sealing. That is a simple way, but the defects or pin-holes inside the inorganic film would affect the character of resisting the transmission of oxygen and humidity. A promising sealing film is compact Al_2O_3 prepared via ALD [165], which has relatively less defects and can be formed at very low temperature with high uniformity. The lowest WVTR of Al_2O_3 compact layer is 1.7×10^{-5} g/(m^2•d) [166]. Another type about multilayer encapsulation normally employs organic films and inorganic films overlapped with each other. The organic layer can block the inorganic layers' defects and improve the resistance property. Multilayer thin-film encapsulation has been successfully applied in organic photoelectric devices. Vitex [167] reported a Barix^{TM} multilayer encapsulation in OLED application; with AlO_x as inorganic layer and a polymer as organic layer, their encapsulation film obtained an extremely low WVTR of 2×10^{-6} g/(m^2•d).

Recently, Weerasinghe et al. [69] reported a systematic research about the encapsulation of flexible PSCs. Based on the structure of PET/IZO/TiO_2/$CH_3NH_3PbI_3$/Spiro-MeOTAD/Ag, Viewbarriers (Mitsubishi Plastic, Inc) was used as the plastic encapsulated film with the WVTR of 5×10^{-3} g/(m^2•d). In the ambient atmosphere ($T < 25$ °C, humidity of 30%–0.80%) for 500 h, three series of devices without encapsulation and with partial encapsulation and complete encapsulation have been investigated (Fig. 11a). The devices without encapsulation quickly degraded in just 100 h and the devices with partial encapsulation were evidently damaged after 400 h. Only the devices with complete encapsulation can maintain most of the initial efficiency after 500 h (Fig. 11d). The results strongly highlight the significance of full encapsulation of flexible PSCs.

8. Prospects on application directions of flexible PSCs

Flexible PSCs, featuring high power-per-weight ratio, favorable bending/compression endurance and extremely low cost due to the compatibility with R2R fabrication, have a great potential to be applied in a broad range of diverse applications. Especially in some special occasions, rigid devices are not competent. First, flexible PSCs can be used as portable power sources for diverse applications, which is especially important for the occasion far from the electricity grid. Portable flexible PSCs could be easily integrated with clothes, bags and tents in the ways shown in Fig. 12(a–c). Second, it is possible for flexible PSCs to get superior power-per-weight ratio with affordable price than other competing

technologies. Though, flexible GaAs solar cells still holds the highest efficiency record, it is more expensive than flexible PSCs. Solar powered unmanned aerial vehicles (UAV) is suggested to have a fast growing market in both civil as well as military applications (Fig. 12d), which especially emphasize the integrated solar panel's power-per-weight ratio. It is thought that the integration of flexible PSCs can largely prolong the flight distance without recharge, which is of critical importance for some special monitoring purpose or attack missions. Third, there should be another potential market for flexible PSCs, which could be very huge. That is Building Integrated Flexible PSCs. Flexible PSCs could be colorful and semitransparent so that they have good decorative effect to replace conventional glass walls (Fig. 12(e)). Its flexibility and its light weight can benefit for its installation on diverse architectures. In comparison to other competing technologies, flexible PSCs is superior in efficiency than flexible amorphous-Si solar cells, and is superior in low-cost than flexible CIGS and GaAs solar cells.

9. Summary and outlook

PSCs as a rising star in next generation photovoltaics, have drawn enough attention from both academic and industrial fields, showing a great possibility of mass production and commercialization in the near future. Because of the low crystallization temperature, the intrinsic bendability and the solution process features of perovskite materials, the research in the field of flexible PSCs has developed very fast since 2013. Up to now, the efficiency record has reached 17.3% [10] in inverted structured PSCs, 16.5% [35] in regular structure PSCs, 13.07% [73] on metal substrate based PSCs, 9.49% [77] in fiber shaped PSCs and 16.8% [10] in ITO-free flexible PSCs. Among different branches of PSCs toward industrialization, flexible PSCs may be the first to find its unique market, since it has intrinsic difference from conventional and rigid crystalline Si based solar cells.

About the flexible substrate materials, plastic films and metal foils show different characters and pose different technical requirements to the fabrication of flexible PSCs. Metal foils is intrinsically opaque which require transparent counter electrodes for light entrance, but their conductivity are better than plastic ones and, more important, they can afford much higher temperature treatment. Nevertheless, for a higher power-per-weight ratio and a simpler manufacture, plastic films have attracted more attention.

On the transparent substrates, ITO coating is conventionally used as conductive photoanode. And in the same time, hindered by ITO coating's brittle property, new conductive and transparent photoanodes have also been explored, such as conductive polymer thin films, metallic meshes, carbon nanotube and graphene based materials. About electron transport interfacial materials, the low-temperature deposition of TiO_2 compact layer has been considerably resolved. In addition, other n-type metal oxides, such as SnO_2, ZnO, Zn_2SnO_4, have been demonstrated as effective alternatives, though ZnO has intrinsic stability problems with respect to perovskites. To use fullerene derivatives as electron transport interfacial material or modifier to n-type metal oxides, normally results in less hysteresis and improved stability. The nanoink strategy for preparing inorganic charge transport layers at low temperature shows a great potential for industrialization. About the hole transport interfacial materials, to replace conventional PEDOT:PSS is important to improve the device efficiency and the stability. NiO_x in comparison to other metal oxides, has been more frequently studied as a hole transport material. Its low-temperature strategy, such as NiO_x nanoink, has been reported with good performance. Recently reported Cu-based inorganic hole transport materials, such as CuI, CuSCN and $CuGaO_2$, are worthy for further development.

In order to realize mass production of flexible PSCs, R2R techniques need to be developed together with the key materials' recent progress. Especially, new techniques to prepare high-quality large area perovskite films are worthy to dedicate more effort in a short term. Currently, the highest efficiency of large area flexible PSC module fabricated by slot die with a printed counter electrode was just 5.4% [104], in view of the big efficiency gap to small area flexible PSCs, there is a big room for further development in this direction. About the stability issue of flexible PSCs, thin film encapsulation techniques emphasizing extremely low WVTR should be considered, which could be learned from the research fields of OLEDs and OPVs. Finally, flexible PSCs can be applied in diverse occasions, if the module efficiency and the stability have been improved to some extent, it is strongly believed that flexible PSCs can find a certain market different from rigid crystalline Si-solar cells.

Acknowledgments

This work was financially supported by the National Natural Science Foundation of China (51672094, 51661135023), the National Key R&D Program of China (2016YFC0205002), the Self-determined and Innovative Research Funds of HUST (2016JCTD111), the open research funds of Engineering Research Center of Nano-Geo Materials of Ministry of Education, China University of Geosciences (NGM2017KF013).

References

[1] REN21,<2016><Renewables Global Status Report 2016>, Paris. http://www.ren21.net/wp-content/uploads/2016/06/GSR_2016_Fig._14.jpg
[2] J.S. Lewis, M.S. Weaver, IEEE J. Sel. Top. Quantum Electron 10 (2004) 45–57.
[3] M. Paggi, I. Berardone, A. Infuso, M. Corrado, Sci. Rep 4 (2014) 4506.
[4] P. Verlinden, A. Blakers, K. Weber, J. Babaei, V. Everett, M. Kerr, M. Stuckings, D. Gordeev, M. Stocks, Sol. Energy Mater. Sol. Cells 90 (2006) 3422–3430.
[5] B.M. Kayes, H. Nie, R. Twist, S.G. Spruytte, F. Reinhardt, I.C. Kizilyalli, G.S., in: Photovoltaic Specialists Conference (PVSC), 37, IEEE, 2011, pp. 000004–000008.
[6] P. Reinhard, A. Chirila, F. Pianezzi, S. Nishiwaki, in: Twentieth International Workshop on Active-Matrix Flatpanel Displays and Devices IEEE, 2013, pp. 79–82.
[7] J.H. Park, Y. Jun, H.G. Yun, S.Y. Lee, M.G. Kang, J. Electrochem. Soc. 155 (2008) 145–149.
[8] J.H. Seo, I. Hwang, H.D. Um, S. Lee, K. Lee, J. Park, H. Shin, T.H. Kwon, S.J. Kang, K. Seo, Adv. Mater. 3 (2017) 1701479.
[9] S. Berny, N. Blouin, A. Distler, H.J. Egelhaaf, M. Krompiec, A. Lohr, O.R. Lozman, G.E. Morse, L. Nanson, A. Pron, Adv. Sci. 3 (2016) 1500342.
[10] J. Yoon, H. Sung, G. Lee, W. Cho, N. Ahn, H.S. Jung, M. Choi, Energy Environ. Sci. 10 (2017) 337–345.
[11] G. Rose, De novis quibusdam fossilibus quae in montibus Uraliis inveniuntur, typis AG Schadii, Berlin, 1839.
[12] A. Salau, Sol. Energy Mater. 2 (1980) 327–332.
[13] A. Kojima, K. Teshima, Y. Shirai, T. Miyasaka, J. Am. Chem. Soc. 131 (2009) 6050–6051.
[14] M.A. Green, A. Ho-Baillie, H.J. Snaith, Nat. Photonics 8 (2014) 506–514.
[15] Y. Ma, S. Wang, L. Zheng, Z. Lu, D. Zhang, Z. Bian, C. Huang, L. Xiao, Chin. J. Chem. 32 (2014) 957–963.
[16] C.C. Stoumpos, C.D. Malliakas, M.G. Kanatzidis, Inorg. Chem. 52 (2013) 9019–9038.
[17] S. Sharma, N. Weiden, A. Weiss, Z. Phys. Chem. 175 (1992) 63–80.
[18] H.S. Kim, C.R. Lee, J.H. Im, K.B. Lee, T. Moehl, A. Marchioro, S.J. Moon, R. Humphry-Baker, J.H. Yum, J.E. Moser, Sci. Rep. 2 (2012) 591.
[19] J.H. Heo, S.H. Im, J.H. Noh, T.N. Mandal, C.S. Lim, J.A. Chang, Y.H. Lee, H.j. Kim, A. Sarkar, M.K. Nazeeruddin, Nat. Photonics 7 (2013) 486–491.
[20] J.W. Lee, D.J. Seol, A.N. Cho, N.G. Park, Adv. Mater. 26 (2014) 4991–4998.
[21] G.E. Eperon, G.M. Paternò, R.J. Sutton, A. Zampetti, A.A. Haghighirad, F. Cacialli, H.J. Snaith, J. Mater. Chem. A 3 (2015) 19688–19695.
[22] M. Kaltenbrunner, G. Adam, E.D. Głowacki, M. Drack, R. Schwödiauer, L. Leonat, D.H. Apaydin, H. Groiss, M.C. Scharber, M.S. White, Nat. Mater. 14 (2015) 1032–1039.
[23] J. Feng, APL. Mater. 2 (2014) 081801.
[24] M. Long, T. Zhang, H. Zhu, G. Li, F. Wang, W. Guo, Y. Chai, W. Chen, Q. Li, K.S. Wong, J. Xu, K. Yan, Nano Energy 33 (2017) 485–496.
[25] M. Long, T. Zhang, Y. Chai, C.-F. Ng, T.C.W. Mak, J. Xu, K. Yan, Nat. Commun. 7 (2016) 13503.
[26] M. Long, T. Zhang, W. Xu, X. Zeng, F. Xie, Q. Li, Z. Chen, F. Zhou, K.S. Wong, K. Yan, J. Xu, Adv. Energy Mater. 7 (2017) 1601882.

[27] K. Yan, M. Long, T. Zhang, Z. Wei, H. Chen, S. Yang, J. Xu, J. Am. Chem. Soc. 137 (2015) 4460–4468.
[28] G.E. Eperon, V.M. Burlakov, P. Docampo, A. Goriely, H.J. Snaith, Adv. Funct. Mater. 24 (2014) 151–157.
[29] H. Zhang, J. Cheng, D. Li, F. Lin, J. Mao, C. Liang, A.K.Y. Jen, M. Grätzel, W.C. Choy, Adv. Mater. 29 (2017) 1604695.
[30] A.T. Barrows, A.J. Pearson, C.K. Kwak, A.D. Dunbar, A.R. Buckley, D.G. Lidzey, Energy Environ. Sci. 7 (2014) 2944–2950.
[31] S.G. Li, K.J. Jiang, M.J. Su, X.P. Cui, J.H. Huang, Q.Q. Zhang, X.Q. Zhou, L.M. Yang, Y.L. Song, J. Mater. Chem. A 3 (2015) 9092–9097.
[32] K. Hwang, Y.S. Jung, Y.J. Heo, F.H. Scholes, S.E. Watkins, J. Subbiah, D.J. Jones, D.Y. Kim, D. Vak, Adv. Mater. 27 (2015) 1241–1247.
[33] Z. Yang, C.C. Chueh, F. Zuo, J.H. Kim, P.W. Liang, A.K.Y. Jen, Adv. Energy. Mater. 5 (2015) 1500328.
[34] M.H. Kumar, N. Yantara, S. Dharani, M. Graetzel, S. Mhaisalkar, P.P. Boix, N. Mathews, Chem. Commun. 49 (2013) 11089–11091.
[35] S.S. Shin, W.S. Yang, E.J. Yeom, S.J. Lee, N.J. Jeon, Y.C. Joo, I.J. Park, J.H. Noh, S.I. Seok, J. Phys. Chem. Lett. 7 (2016) 1845–1851.
[36] P. Docampo, J.M. Ball, M. Darwich, G.E. Eperon, H.J. Snaith, Nat. Commun. 4 (2013) 2761.
[37] V. Zardetto, T.M. Brown, A. Reale, A. Di Carlo, J. Polym, Sci. Pt. B-Polym. Phys. 49 (2011) 638–648.
[38] J.I. Park, J.H. Heo, S.H. Park, K.I. Hong, H.G. Jeong, S.H. Im, H.K. Kim, J. Power Sources 341 (2017) 340–347.
[39] F. Di Giacomo, A. Fakharuddin, R. Jose, T.M. Brown, Energy Environ. Sci. 9 (2016) 3007–3035.
[40] B.A. Nejand, P. Nazari, S. Gharibzadeh, V. Ahmadi, A. Moshaii, Chem. Commun. 53 (2017) 747–750.
[41] L. Qiu, J. Deng, X. Lu, Z. Yang, H. Peng, Angew. Chem.-Int. Ed. 53 (2014) 10425–10428.
[42] S. He, L. Qiu, X. Fang, G. Guan, P. Chen, Z. Zhang, H. Peng, J. Mater. Chem. A 3 (2015) 9406–9410.
[43] M. Park, H.J. Kim, I. Jeong, J. Lee, H. Lee, H.J. Son, D.E. Kim, M.J. Ko, Adv. Energy Mater. 5 (2015) 1501406.
[44] M.M. Tavakoli, K.H. Tsui, Q. Zhang, J. He, Y. Yao, D. Li, Z. Fan, ACS Nano 9 (2015) 10287–10295.
[45] H.G. Im, S. Jeong, J. Jin, J. Lee, D.Y. Youn, W.T. Koo, S.B. Kang, H.J. Kim, J. Jang, D. Lee, NPG Asia Mater. 8 (2016) e282.
[46] Y. Zhou, K. Zhu, ACS Energy Lett. 1 (2016) 64–67.
[47] T. Minami, H. Sonohara, T. Kakumu, S. Takata, Thin Solid Films 270 (1995) 37–42.
[48] F.C. Krebs, T. Tromholt, M. Jørgensen, Nanoscale 2 (2010) 873–886.
[49] B.J. Kim, D.H. Kim, Y.Y. Lee, H.W. Shin, G.S. Han, J.S. Hong, K. Mahmood, T.K. Ahn, Y.C. Joo, K.S. Hong, Energy Environ. Sci. 8 (2015) 916–921.
[50] Y.H. Kim, C. Sachse, M.L. Machala, C. May, L. Müller-Meskamp, K. Leo, Adv. Funct. Mater. 21 (2011) 1076–1081.
[51] L. Chen, X. Xie, Z. Liu, E.C. Lee, J. Mater. Chem. A 5 (2017) 6974–6980.
[52] Y. Li, L. Meng, Y.M. Yang, G. Xu, Z. Hong, Q. Chen, J. You, G. Li, Y. Yang, Y. Li, Nat. Commun. 7 (2016) 75–81.
[53] Z. Liu, P. You, C. Xie, G. Tang, F. Yan, Nano Energy 28 (2016) 151–157.
[54] X. Wang, Z. Li, W. Xu, S.A. Kulkarni, S.K. Batabyal, S. Zhang, A. Cao, L.H. Wong, Nano Energy 11 (2015) 728–735.
[55] C. Roldán-Carmona, O. Malinkiewicz, R. Betancur, G. Longo, C. Momblona, F. Jaramillo, L. Camacho, H.J. Bolink, Energy Environ. Sci. 7 (2014) 2968–2973.
[56] M. Lee, Y. Jo, D.S. Kim, Y. Jun, J. Mater. Chem. A 3 (2015) 4129–4133.
[57] M. Lee, Y. Jo, D.S. Kim, H.Y. Jeong, Y. Jun, J. Mater. Chem. A 3 (2015) 14592–14597.
[58] J. Troughton, D. Bryant, K. Wojciechowski, M.J. Carnie, H. Snaith, D.A. Worsley, T.M. Watson, J. Mater. Chem. A 3 (2015) 9141–9145.
[59] R. Li, X. Xiang, X. Tong, J. Zou, Q. Li, Adv. Mater. 27 (2015) 3831–3835.
[60] L. Qiu, S. He, J. Yang, J. Deng, H. Peng, Small 12 (2016) 2419–2424.
[61] K. Poorkazem, D. Liu, T.L. Kelly, J. Mater. Chem. A 3 (2015) 9241–9248.
[62] K. Sun, P. Li, Y. Xia, J. Chang, J. Ouyang, ACS Appl. Mater. Interfaces 7 (2015) 15314–15320.
[63] M. Dianetti, F. Di Giacomo, G. Polino, C. Ciceroni, A. Liscio, A. D'Epifanio, S. Licoccia, T. Brown, A. Di Carlo, F. Brunetti, Sol. Energy Mater. Sol. Cells 140 (2015) 150–157.
[64] C. Roldán-Carmona, O. Malinkiewicz, A. Soriano, G.M. Espallargas, A. Garcia, P. Reinecke, T. Kroyer, M.I. Dar, M.K. Nazeeruddin, H.J. Bolink, Energy Environ. Sci. 7 (2014) 994–997.
[65] I. Jeon, T. Chiba, C. Delacou, Y. Guo, A. Kaskela, O. Reynaud, E.I. Kauppinen, S. Maruyama, Y. Matsuo, Nano Lett. 15 (2015) 6665–6671.
[66] H. Lu, J. Sun, H. Zhang, S. Lu, W.C. Choy, Nanoscale 8 (2016) 5946–5953.
[67] F. Qin, J. Tong, R. Ge, B. Luo, F. Jiang, T. Liu, Y. Jiang, Z. Xu, L. Mao, W. Meng, J. Mater. Chem. A 4 (2016) 14017–14024.
[68] S. Pisoni, F. Fu, T. Feurer, M. Makha, B. Bissig, S. Nishiwaki, A. Tiwari, S. Buecheler, J. Mater. Chem. A 5 (2017) 13639–13647.
[69] H.C. Weerasinghe, Y. Dkhissi, A.D. Scully, R.A. Caruso, Y.B. Cheng, Nano Energy 18 (2015) 118–125.
[70] M. Xu, J. Feng, Z.J. Fan, X.L. Ou, Z.Y. Zhang, H.Y. Wang, H.B. Sun, Sol. Energy Mater. Sol. Cells 169 (2017) 8–12.
[71] X.L. Ou, J. Feng, M. Xu, H.B. Sun, Opt. Lett. 42 (2017) 1958–1961.
[72] M. Lee, Y. Ko, B.K. Min, Y. Jun, ChemSusChem 9 (2016) 31–35.
[73] Y. Xiao, G. Han, H. Zhou, J. Wu, RSC Adv. 6 (2016) 2778–2784.
[74] M. Lee, Y. Ko, Y. Jun, J. Mater. Chem. A 3 (2015) 19310–19313.
[75] J. Deng, L. Qiu, X. Lu, Z. Yang, G. Guan, Z. Zhang, H. Peng, J. Mater. Chem. A 3 (2015) 21070–21076.
[76] H. Hu, K. Yan, M. Peng, X. Yu, S. Chen, B. Chen, B. Dong, X. Gao, D. Zou, J. Mater. Chem. A 4 (2016) 3901–3906.
[77] L. Qiu, S. He, J. Yang, F. Jin, J. Deng, H. Sun, X. Cheng, G. Guan, X. Sun, H. Zhao, J. Mater. Chem. A 4 (2016) 10105–10109.
[78] X. Wang, S.A. Kulkarni, Z. Li, W. Xu, S.K. Batabyal, S. Zhang, A. Cao, L.H. Wong, Nanotechnology 27 (2016) 20LT01.
[79] H.S. Jung, N.G. Park, Small 11 (2015) 10–25.
[80] P.P. Boix, K. Nonomura, N. Mathews, S.G. Mhaisalkar, Mater. Today 17 (2014) 16–23.
[81] F. Di Giacomo, V. Zardetto, A. D'Epifanio, S. Pescetelli, F. Matteocci, S. Razza, A. Di Carlo, S. Licoccia, W.M. Kessels, M. Creatore, T.M. Brown, Adv. Energy Mater. 5 (2015) 1401808.
[82] W. Qiu, U.W. Paetzold, R. Gehlhaar, V. Smirnov, H.G. Boyen, J.G. Tait, B. Conings, W. Zhang, C.B. Nielsen, I. McCulloch, J. Mater. Chem. A 3 (2015) 22824–22829.
[83] D. Yang, R. Yang, J. Zhang, Z. Yang, S.F. Liu, C. Li, Energy Environ. Sci. 8 (2015) 3208–3214.
[84] S.S. Mali, C.K. Hong, A. Inamdar, H. Im, S.E. Shim, Nanoscale 9 (2017) 3095–3104.
[85] I. Jeong, H. Jung, M. Park, J.S. Park, H.J. Son, J. Joo, J. Lee, M.J. Ko, Nano Energy 28 (2016) 380–389.
[86] S.Y. Lin, T.S. Su, T.Y. Hsieh, P.C. Lo, T.C. Wei, Adv. Energy Mater. (2017) 1700169.
[87] A. Yella, L.P. Heiniger, P. Gao, M.K. Nazeeruddin, M. Graẗzel, Nano Lett. 14 (2014) 2591–2596.
[88] H. Tan, A. Jain, O. Voznyy, X. Lan, F.P.G. de Arquer, J.Z. Fan, R. Quintero-Bermudez, M. Yuan, B. Zhang, Y. Zhao, Science 355 (2017) 722–726.
[89] A. Kogo, M. Ikegami, T. Miyasaka, Chem. Commun. 52 (2016) 8119–8122.
[90] K. Keis, E. Magnusson, H. Lindström, S.E. Lindquist, A. Hagfeldt, Sol. Energy Mater. Sol. Cells 73 (2002) 51–58.
[91] A.S. Goncalves, M.S. Goes, F. Fabregat-Santiago, T. Moehl, M.R. Davolos, J. Bisquert, S. Yanagida, A.F. Nogueira, P.R. Bueno, Electrochim. Acta 56 (2011) 6503–6509.
[92] C. Xu, X.W. Sun, Z.L. Dong, G. Zhu, Y. Cui, Appl. Phys. Lett. 88 (2006) 093101.
[93] J.H. Heo, M.H. Lee, H.J. Han, B.R. Patil, J.S. Yu, S.H. Im, J. Mater. Chem. A 4 (2016) 1572–1578.
[94] D. Liu, T.L. Kelly, Nat. Photonics 8 (2014) 133–138.
[95] J. You, L. Meng, T.B. Song, T.F. Guo, W.h. Chang, Z. Hong, H. Chen, H. Zhou, Q. Chen, Y. Liu, Nat. Nanotechnol. 11 (2016) 75.
[96] J. Yang, B.D. Siempelkamp, E. Mosconi, F. De Angelis, T.L. Kelly, Chem. Mater. 27 (2015) 4229–4236.
[97] S.S. Shin, D.W. Kim, D. Hwang, J.H. Suk, L.S. Oh, B.S. Han, D.H. Kim, J.S. Kim, D. Kim, J.Y. Kim, ChemSusChem 7 (2014) 501–509.
[98] S.S. Shin, W.S. Yang, J.H. Noh, J.H. Suk, N.J. Jeon, J.H. Park, J.S. Kim, W.M. Seong, S.I. Seok, Nat. Commun. 6 (2015) 7410.
[99] H.L. Yip, A.K.Y. Jen, Energy Environ. Sci. 5 (2012) 5994–6011.
[100] Y. Shao, Z. Xiao, C. Bi, Y. Yuan, J. Huang, Nat. Commun. 5 (2014) 5784.
[101] J. You, Z. Hong, Y.M. Yang, Q. Chen, M. Cai, T.B. Song, C.C. Chen, S. Lu, Y. Liu, H. Zhou, ASC Nano 8 (2014) 1674–1680.
[102] J.W. Jung, S.T. Williams, A.K.Y. Jen, RSC Adv. 4 (2014) 62971–62977.
[103] Y.F. Chiang, J.Y. Jeng, M.H. Lee, S.R. Peng, P. Chen, T.F. Guo, T.C. Wen, Y.J. Hsu, C.M. Hsu, Phys. Chem. Chem. Phys. 16 (2014) 6033–6040.
[104] T.M. Schmidt, T.T. Larsen-Olsen, J.E. Carlé, D. Angmo, F.C. Krebs, Adv. Energy Mater. 5 (2015) 1500569.
[105] S. Ryu, J. Seo, S.S. Shin, Y.C. Kim, N.J. Jeon, J.H. Noh, S.I. Seok, J. Mater. Chem. A 3 (2015) 3271–3275.
[106] P.W. Dunk, A. Rodríguez-Fortea, N.K. Kaiser, H. Shinohara, J.M. Poblet, H.W. Kroto, Angew. Chem. 125 (2013) 333–337.
[107] P.W. Liang, C.C. Chueh, S.T. Williams, A.K.Y. Jen, Adv. Energy Mater. 5 (2015) 1402321.
[108] K. Wojciechowski, T. Leijtens, S. Siprova, C. Schlueter, M.T. Hoïantner, J.T.W. Wang, C.Z. Li, A.K.Y. Jen, T.L. Lee, H.J. Snaith, J. Phys. Chem. Lett. 6 (2015) 2399–2405.
[109] W. Ke, D. Zhao, C.R. Grice, A.J. Cimaroli, J. Ge, H. Tao, H. Lei, G. Fang, Y. Yan, J. Mater. Chem. A 3 (2015) 17971–17976.
[110] H. Yoon, S.M. Kang, J.K. Lee, M. Choi, Energy Environ. Sci. 9 (2016) 2262–2266.
[111] K. Wang, Y. Shi, L. Gao, R. Chi, K. Shi, B. Guo, L. Zhao, T. Ma, Nano Energy 31 (2017) 424–431.
[112] J. Feng, Z. Yang, D. Yang, X. Ren, X. Zhu, Z. Jin, W. Zi, Q. Wei, S.F. Liu, Nano Energy 36 (2017) 1–8.
[113] M. Park, J.Y. Kim, H.J. Son, C.H. Lee, S.S. Jang, M.J. Ko, Nano Energy 26 (2016) 208–215.
[114] Z. Zhu, J.Q. Xu, C.C. Chueh, H. Liu, Z.a. Li, X. Li, H. Chen, A.K.Y. Jen, Adv. Mater. 28 (2016) 10786–10793.
[115] T. Torimoto, T. Tsuda, K.i. Okazaki, S. Kuwabata, Adv. Mater. 22 (2010) 1196–1221.
[116] Q. Jiang, L. Zhang, H. Wang, X. Yang, J. Meng, H. Liu, Z. Yin, J. Wu, X. Zhang, J. You, Nat. Energy 2 (2016) 16177.
[117] M. Long, Z. Chen, T. Zhang, Y. Xiao, X. Zeng, J. Chen, K. Yan, J. Xu, Nanoscale 8 (2016) 6290–6299.
[118] A. Abate, T. Leijtens, S. Pathak, J. Teuscher, R. Avolio, M.E. Errico, J. Kirkpatrik, J.M. Ball, P. Docampo, I. McPherson, Phys. Chem. Chem. Phys. 15 (2013) 2572–2579.
[119] R. Scholin, M.H. Karlsson, S.K. Eriksson, H. Siegbahn, E.M. Johansson, H. Rensmo, J. Phys. Chem. C 116 (2012) 26300–26305.

[120] Y. Yue, N. Salim, Y. Wu, X. Yang, A. Islam, W. Chen, J. Liu, E. Bi, F. Xie, M. Cai, Adv. Mater. 28 (2016) 10738–10743.
[121] Z. Li, C. Xiao, Y. Yang, S.P. Harvey, D.H. Kim, J.A. Christians, M. Yang, P. Schulz, S.U. Nanayakkara, C.S. Jiang, Energy Environ. Sci. 10 (2017) 1234–1242.
[122] F. Hou, Z. Su, F. Jin, X. Yan, L. Wang, H. Zhao, J. Zhu, B. Chu, W. Li, Nanoscale 7 (2015) 9427–9432.
[123] J.H. Kim, P.W. Liang, S.T. Williams, N. Cho, C.C. Chueh, M.S. Glaz, D.S. Ginger, A.K.Y. Jen, Adv. Mater. 27 (2015) 695–701.
[124] W. Guo, K. Hui, K.S. Hui, Mater. Lett. 92 (2013) 291–295.
[125] M.D. Irwin, D.B. Buchholz, A.W. Hains, R.P. Chang, T.J. Marks, Proc. Natl. Acad. Sci. USA 105 (2008) 2783–2787.
[126] J.Y. Jeng, K.C. Chen, T.Y. Chiang, P.Y. Lin, T.D. Tsai, Y.C. Chang, T.F. Guo, P. Chen, T.C. Wen, Y.J. Hsu, Adv. Mater. 26 (2014) 4107–4113.
[127] J.H. Park, J. Seo, S. Park, S.S. Shin, Y.C. Kim, N.J. Jeon, H.W. Shin, T.K. Ahn, J.H. Noh, S.C. Yoon, Adv. Mater. 27 (2015) 4013–4019.
[128] J. Cui, F. Meng, H. Zhang, K. Cao, H. Yuan, Y. Cheng, F. Huang, M. Wang, ACS Appl. Mater. Interfaces 6 (2014) 22862–22870.
[129] J.I. Park, J.H. Heo, S.H. Park, K.I. Hong, H.G. Jeong, S.H. Im, H.K. Kim, J. Power Sources 341 (2017) 340–347.
[130] X. Yin, P. Chen, M. Que, Y. Xing, W. Que, C. Niu, J. Shao, ACS Nano 10 (2016) 3630–3636.
[131] Z. Liu, A. Zhu, F. Cai, L. Tao, Y. Zhou, Z. Zhao, Q. Chen, Y.-B. Cheng, H. Zhou, J. Mater. Chem. A 5 (2017) 6597–6605.
[132] J.W. Jung, J.S. Park, I.K. Han, Y. Lee, C. Park, W. Kwon, M. Park, J. Mater. Chem. A 24 (2017) 12158–12167.
[133] M. Park, J.S. Park, I.K. Han, J.Y. Oh, J. Mater. Chem. A 4 (2016) 11307–11316.
[134] J.W. Jo, M.S. Seo, M. Park, J.Y. Kim, J.S. Park, I.K. Han, H. Ahn, J.W. Jung, B.H. Sohn, M.J. Ko, Adv. Funct. Mater. 26 (2016) 4464–4471.
[135] H. Zhang, H. Wang, W. Chen, A.K.Y. Jen, Adv. Mater. 29 (2017) 1604984.
[136] S. Das, B. Yang, G. Gu, P.C. Joshi, I.N. Ivanov, C.M. Rouleau, T. Aytug, D.B. Geohegan, K. Xiao, ACS Photonics 2 (2015) 680–686.
[137] V. Zardetto, F. Di Giacomo, G. Lucarelli, W. Kessels, T. Brown, M. Creatore, Sol. Energy 150 (2017) 447–453.
[138] G. Lucarelli, F. Di Giacomo, V. Zardetto, M. Creatore, T.M. Brown, Nano Res. 10 (2017) 2130–2145.
[139] H. Zhou, Y. Shi, K. Wang, Q. Dong, X. Bai, Y. Xing, Y. Du, T. Ma, J. Phys. Chem. C 119 (2015) 4600–4605.
[140] S. Ameen, M.S. Akhtar, H.K. Seo, M.K. Nazeeruddin, H.S. Shin, J. Phys. Chem. C 119 (2015) 10379–10390.
[141] M.M. Tavakoli, Q. Lin, S.F. Leung, G.C. Lui, H. Lu, L. Li, B. Xiang, Z. Fan, Nanoscale 8 (2016) 4276–4283.
[142] X. Liu, C.C. Chueh, Z. Zhu, S.B. Jo, Y. Sun, A.K.-Y. Jen, J. Mater. Chem. A 4 (2016) 15294–15301.
[143] H. Kim, C.C. Chueh, S.T. Williams, A.K.Y. Jen, Nanoscale 7 (2015) 17343–17349.
[144] S. Ameen, M.S. Akhtar, H.K. Seo, M.K. Nazeeruddin, H.S. Shin, Dalton Trans. 44 (2015) 6439–6448.
[145] J. Wei, H. Li, Y. Zhao, W. Zhou, R. Fu, H. Pan, Q. Zhao, Chem. Commun. 52 (2016) 10791–10794.
[146] Z. Chen, G. Yang, X. Zheng, H. Lei, C. Chen, J. Ma, H. Wang, G. Fang, J. Power Sources 351 (2017) 123–129.
[147] J. Ha, H. Kim, H. Lee, K.G. Lim, T.W. Lee, S. Yoo, Sol. Energy Mater. Sol. Cells 161 (2017) 338–346.
[148] X. Xu, Q. Chen, Z. Hong, H. Zhou, Z. Liu, W.H. Chang, P. Sun, H. Chen, N.D. Marco, M. Wang, Nano Lett. 15 (2015) 6514–6520.
[149] L.L. Gao, L.S. Liang, X.X. Song, B. Ding, G.J. Yang, B. Fan, C.X. Li, C.J. Li, J. Mater. Chem. A 4 (2016) 3704–3710.
[150] Y. Chen, T. Chen, L. Dai, Adv. Mater. 27 (2015) 1053–1059.
[151] Y. Chen, Y. Zhao, Z. Liang, Chem. Mater. 27 (2015) 1448–1451.
[152] Z. Gu, L. Zuo, T.T. Larsen-Olsen, T. Ye, G. Wu, F.C. Krebs, H. Chen, J. Mater. Chem. A 3 (2015) 24254–24260.
[153] K. Yao, X. Wang, Y.X. Xu, F. Li, Nano Energy 18 (2015) 165–175.
[154] H. Wu, C. Zhang, K. Ding, L. Wang, Y. Gao, J. Yang, Org. Electron. 45 (2017) 302–307.
[155] J. Xi, Z. Wu, B. Jiao, H. Dong, C. Ran, C. Piao, T. Lei, T.B. Song, W. Ke, T. Yokoyama, Adv. Mater. 29 (2017) 1606964.
[156] Z. Yang, S. Zhang, L. Li, W. Chen, J. Materiomics 3 (2017) 231–244.
[157] J. Ciro, M.A. Mejía-Escobar, F. Jaramillo, Sol. Energy 150 (2017) 570–576.
[158] Y. Zhang, X. Hu, L. Chen, Z. Huang, Q. Fu, Y. Liu, L. Zhang, Y. Chen, Org. Electron. 30 (2016) 281–288.
[159] S.H. Ahn, L.J. Guo, Adv. Mater. 20 (2008) 2044–2049.
[160] Z. Yang, W. Ahmad, L. Chu, M.R. Al-bahrani, F. Tu, Y. Wang, H. Zhang, X. Wang, J. Su, N. Liu, L. Li, C. Yang, Y. Gao, RSC Adv. 6 (2016) 55071–55078.
[161] J.H. Noh, S.H. Im, J.H. Heo, T.N. Mandal, S.I. Seok, Nano Lett. 13 (2013) 1764–1769.
[162] Q. Jiang, D. Rebollar, J. Gong, E.L. Piacentino, C. Zheng, T. Xu, Angew. Chem. 127 (2015) 7727–7730.
[163] Y. Han, S. Meyer, Y. Dkhissi, K. Weber, J.M. Pringle, U. Bach, L. Spiccia, Y.-B. Cheng, J. Mater. Chem. A 3 (2015) 8139–8147.
[164] https://static.thermoscientific.com.
[165] A. Ghosh, L. Gerenser, C. Jarman, J. Fornalik, Appl. Phys. Lett. 86 (2005) 223503.
[166] P. Carcia, R. McLean, M. Reilly, M. Groner, S. George, Appl. Phys. Lett. 89 (2006) 031915.
[167] G. Nisato, M. Kuilder, P. Bouten, L. Moro, O. Philips, N. Rutherford, SID Symp. Dig. Tech. Pap. 34 (2013) 550–553.
[168] Z. Chai, N. Zhang, P. Sun, Y. Huang, C. Zhao, H.J. Fan, X. Fan, W. Mai, ACS Nano 10 (2016) 9201–9207.
[169] http://blog.thesietch.org/2007/06/22/early-morning-solar-gadget-the-mana-solar-claw/.
[170] http://www.tacticalsolar.com/rugged_solar_tents.php.
[171] http://www.silentfalconuas.com/silent-falcon.
[172] http://www.belectric.co.uk/1348-2/.